5-2011

UV, Optical, and Infrared Imaging of the Interacting Galaxy Arp 107 and its Star Forming Regions.

Ryen C. Lapham

East Tennessee State University

UV, Optical, and Infrared Imaging of the
Interacting Galaxy Arp 107 and
its Star Forming Regions

Ryen C. Lapham

Department of Physics and Astronomy, East Tennessee State University, Johnson City, TN

37614

Received ⎯⎯⎯⎯⎯⎯⎯⎯; accepted ⎯⎯⎯⎯⎯⎯⎯⎯

An honors thesis presented to the faculty of the Department of Physics and Astronomy at East Tennessee State University in partial fulfillment of the requirements for the Honors Scholars Program.

ABSTRACT

In this study we present GALEX UV, Sloan Digital Sky Survey, and Spitzer infrared imaging, along with an optical Hα map of the interacting galaxy pair Arp 107. IRAF photometry was used to analyze 29 star forming regions identified in previous work done with Spitzer colors. In this paper further analysis of the clumps of newly formed stars was done by creating Spectral Energy Distribution plots to sort the clumps as quiescent or starbursts. Color - color plots were used to estimate the ages and extinctions of the clumps by comparing magnitudes to stellar population synthesis models. Results seem to agree with previous models, and indicate a sequence of increasing age around the galaxy arm.

Subject headings: galaxies: indiviual (Arp 107)–galaxies: interactions–galaxies: starburst

1. Introduction

Galaxy interactions, collisions, and mergers play a major role in the evolution of galaxies, greatly affecting the morphology and star formation rates of interacting galaxies (Struck 1999). Much work is being done to study the effects of galaxy interactions, and there is plenty of observational and modeling information to be utilized. Numerous galaxy pairs have been selected from the Arp Atlas of Peculiar Galaxies to be analyzed (Arp 1966). Previous work includes detailed studies of Arp 82 (Hancock et al. 2007), Arp 285 (Smith et al. 2008), and Arp 305 (Hancock et al. 2009), as well as broader studies done with the Galaxy Evolution Explorer (GALEX), Sloan Digitized Sky Survey (SDSS), and Spitzer images (Smith et al. 2007).

The information presented in these papers is consistent with and shows that galaxy interactions produce clumps of star forming regions in various ways. Arp 285 and Arp 82 have examples of "beads on a string", clumps separated by a characteristic distance scale of 1 kpc. Arp 305 contains a Tidal Dwarf Galaxy along a bridge between its interacting galaxies, as well as an oval shaped star forming region shaped like an eyelid. This type of feature is seen in Arp 82 as well and is assumed to be the result of large-scale gaseous shocks from a grazing prograde encounter (Hancock et al. 2009). Color comparisons done with GALEX and SDSS images indicate enhanced star formation in tidal features, showing tails and bridges to be more prominent in the UV images as opposed to their parent disks (Smith et al. 2010). Spitzer images also provide evidence for enhanced star formation in pre-merger interacting galaxy pairs. The Spitzer infrared colors of the interacting galaxies selected for the study are redder on average than normal spirals, and imply an enhancement to the mass-normalized star formation rate of a factor of two (Smith et al. 2007).

The interacting galaxy pair Arp 107 is characterized by a large spiral arm in the southern part of the larger galaxy and a bridge towards its companion in the northeast.

Arp 107 was previously studied in the infrared using Spitzer data (Smith et al. 2005). The primary spiral arm contains several clumps whose [3.6] - [4.5] color is consistent with that of stars. However there is variation in the [4.5] - [5.8] colors with a clear azimuthal sequence around the arm, implying a sequence in the age of the stars in these clumps. A large variation in the [3.6] - [8.0] color was observed as well, but is mainly due to changes in the [4.5] - [5.8] color. Attempts at modeling the interaction have shown Arp 107 to be an off-center collision somewhere between a ring model and a tidal model (Smith et al. 2005). The pattern of ages around the spiral arm may be explained by models as the result of differences in the time of maximum compression in the spiral arm (Smith et al. 2005).

2. Observations

The images used to study Arp 107 come from GALEX, SDSS, and Spitzer data, and the data we are using were previously presented in Smith et al. (2010), Abazajian et al. (2003), and Fazio et al. (2004), respectively. Arp 107 is at a distance of 138 Mpc (Keel et al. 1985), assuming $H_0 = 75$ km/s/Mpc. The larger galaxy in the pair has a Seyfert 2 nucleus (Keel et al. 1985). Arp 107 was imaged with GALEX in both the far-UV (FUV) and near-UV (NUV) bands. The images have a pixel size of 1".5 and a circular field of view with a diameter of 1.2 degrees. The NUV band covers 1750-2800 Angstroms while the FUV band covers 1350-1705 Angstroms. The images were taken between 7 April 2005 and 25 March 2006. The total imaging time for the FUV and NUV filters is 1094 seconds and 2610 seconds, respectively.

The SDSS images have a pixel size of 0.4" and a field of view of 13'.5 x 9'.8. Wavelengths vary among the ugriz optical filters with the u, g, r, i, and z filters having effective wavelengths 3560, 4680, 6180, 7500, and 8870 Angstroms, respectively.
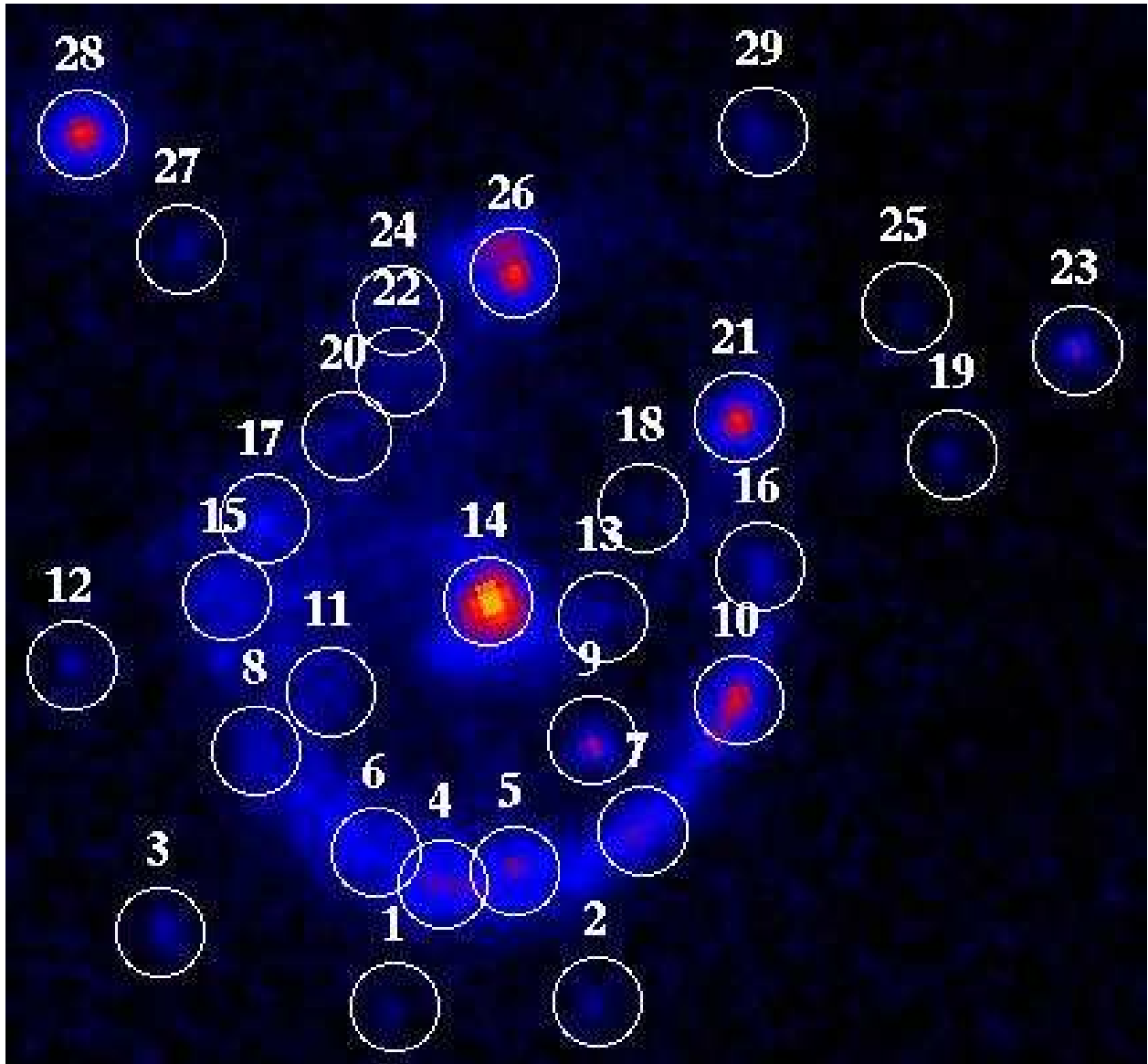
Fig. 1.— 29 clumps are identified in the Spitzer 8.0 μm image of Arp 107 with 5" radius circles. The clumps are numbered in order of increasing declination. This image comes from Smith et al. (2005)

Arp 107 was imaged by the Spitzer Infrared Array Camera on 2004 December 17 in the 3.6, 4.5, 5.8, and 8.0 μm broadband filters. Exposures were 12 s each, with 23 exposures per filter, giving a total integration time 276 s per filter. The images have a pixel size of 1".2 and a field of view of 9'.0 x 14'.8, with the long axis at a position angle of 19.8 degrees east of north.

Optical images were taken with the 0.6 m Erwin Fick Telescope in Boone, Iowa, on 2005 April 8, 14, 15 under clear, dark skies. Seven 450 s images in a redshifted Hα filter were taken and reduced in the standard way with the Image Reduction and Analysis Facility (IRAF) sofware. The Spitzer and Hα images were previously published in Smith et al. (2005).

Aperture photometry was done with the IRAF phot command, using an aperture size of 5 scale units and a mode sky fitting algorithm with an inner annulus of 6 scale units and an outer annulus of 12 scale units. The results are listed in Table 1. The Right Ascension and Declination of each clump can be found in Smith et al. (2005). Aperture corrections and were done manually for the GALEX and SDSS images by taking counts of three moderately bright field stars and slowly increasing the radius until the counts leveled off. For the FUV and NUV wavelengths the aperture corrections were 1.43 and 1.42, respectively. The SDSS u, g, r, i, and z filters were found to need no aperture corrections, except for the z band which needed a correction of 1.002. These values were compared to aperture corrections found in Hancock et al. (2009) for GALEX and SDSS images and were similiar. For the Spitzer images, aperture corrections were used as listed in the IRAC Data Manual. They are 1.06, 1.06, 1.07, and 1.09 for the 3.6, 4.5, 5.8, and 8.0 μm wavelengths, respectively.

Table 1.   Magnitudes and Hα Fluxes for Clumps in Arp 107

ID	FUV	NUV	u	g	r	i	z	3.6 μm	4.5 μm	5.8 μm	8.0 μm	Hα
1	23.2 ± 0.0	23.5 ± 0.2	–	–	21.6 ± 0.4	–	–	15.9 ± 0.0	15.9 ± 0.0	16.1 ± 0.3	14.7 ± 0.1	–
2	22.1 ± 0.0	22.3 ± 0.1	–	19.9 ± 0.1	19.1 ± 0.0	18.9 ± 0.1	19.3 ± 0.3	16.4 ± 0.0	16.3 ± 0.1	15.8 ± 0.2	14.2 ± 0.1	0.02 ± 0.17
3	23.0 ± 0.0	22.5 ± 0.1	–	20.6 ± 0.1	19.6 ± 0.1	19.0 ± 0.1	18.7 ± 0.1	15.8 ± 0.0	15.6 ± 0.0	15.6 ± 0.2	14.0 ± 0.1	–
4	20.3 ± 0.0	20.0 ± 0.0	19.8 ± 0.1	18.3 ± 0.0	17.9 ± 0.0	17.8 ± 0.0	17.6 ± 0.1	15.0 ± 0.1	15.0 ± 0.1	13.6 ± 0.0	11.7 ± 0.0	1.56 ± 0.19
5	20.4 ± 0.0	20.2 ± 0.0	19.8 ± 0.1	18.6 ± 0.0	18.1 ± 0.0	17.9 ± 0.0	18.0 ± 0.1	15.2 ± 0.1	15.1 ± 0.1	13.7 ± 0.1	11.8 ± 0.0	2.79 ± 0.19
6	20.5 ± 0.0	20.0 ± 0.0	19.6 ± 0.1	18.2 ± 0.0	17.8 ± 0.0	17.6 ± 0.0	17.5 ± 0.1	15.0 ± 0.1	15.0 ± 0.1	13.9 ± 0.1	12.1 ± 0.0	0.49 ± 0.19
7	20.3 ± 0.0	20.0 ± 0.0	20.1 ± 0.1	18.7 ± 0.0	18.4 ± 0.0	18.1 ± 0.0	18.0 ± 0.1	15.3 ± 0.1	15.4 ± 0.1	13.8 ± 0.1	12.0 ± 0.0	2.44 ± 0.19
8	20.8 ± 0.0	20.5 ± 0.0	21.2 ± 0.3	19.1 ± 0.0	18.9 ± 0.1	18.9 ± 0.1	19.1 ± 0.2	15.6 ± 0.1	15.7 ± 0.1	15.0 ± 0.2	12.7 ± 0.1	0.76 ± 0.18
9	–	–	–	18.3 ± 0.0	16.7 ± 0.0	15.8 ± 0.0	15.3 ± 0.0	13.1 ± 0.0	13.1 ± 0.0	13.1 ± 0.0	13.2 ± 0.1	–
10	19.4 ± 0.0	19.3 ± 0.0	19.2 ± 0.1	18.7 ± 0.0	18.6 ± 0.0	18.4 ± 0.0	18.6 ± 0.1	15.5 ± 0.1	15.4 ± 0.1	13.5 ± 0.0	11.6 ± 0.0	14.36 ± 0.20
11	21.9 ± 0.1	22.4 ± 0.3	–	21.0 ± 0.2	20.1 ± 0.2	19.8 ± 0.2	19.0 ± 0.2	16.7 ± 0.3	17.0 ± 0.3	–	14.4 ± 0.3	–
12	22.6 ± 0.0	21.6 ± 0.0	19.9 ± 0.1	18.5 ± 0.0	17.9 ± 0.0	17.6 ± 0.0	17.3 ± 0.0	14.9 ± 0.0	14.8 ± 0.0	14.7 ± 0.1	13.9 ± 0.1	–
13	23.2 ± 0.3	–	–	20.7 ± 0.1	20.1 ± 0.1	19.8 ± 0.1	–	16.0 ± 0.1	16.1 ± 0.1	15.3 ± 0.2	13.7 ± 0.1	2.08 ± 0.21
14	20.6 ± 0.0	20.2 ± 0.0	18.5 ± 0.0	16.7 ± 0.0	15.9 ± 0.0	15.4 ± 0.0	15.1 ± 0.0	12.5 ± 0.0	12.5 ± 0.0	11.9 ± 0.0	10.5 ± 0.0	52.63 ± 0.19
15	20.7 ± 0.0	20.4 ± 0.0	20.4 ± 0.2	19.4 ± 0.1	19.5 ± 0.1	19.2 ± 0.1	18.9 ± 0.2	15.7 ± 0.1	15.8 ± 0.1	14.6 ± 0.1	12.7 ± 0.1	0.88 ± 0.20
16	21.0 ± 0.0	21.1 ± 0.0	20.5 ± 0.2	20.5 ± 0.1	19.9 ± 0.1	19.7 ± 0.1	–	17.1 ± 0.2	17.1 ± 0.2	15.8 ± 0.2	13.4 ± 0.1	3.28 ± 0.18
17	20.9 ± 0.0	20.6 ± 0.0	20.5 ± 0.2	19.4 ± 0.1	18.9 ± 0.1	18.8 ± 0.1	18.6 ± 0.1	15.6 ± 0.1	15.8 ± 0.1	14.9 ± 0.1	13.0 ± 0.1	0.55 ± 0.18
18	23.2 ± 0.3	–	–	–	–	–	–	–	–	–	15.2 ± 0.4	0.46 ± 0.21
19	23.6 ± 0.0	–	–	–	–	–	–	17.2 ± 0.1	16.7 ± 0.1	15.6 ± 0.2	14.4 ± 0.1	–
20	22.9 ± 0.2	23.1 ± 0.3	–	20.6 ± 0.1	19.7 ± 0.1	19.6 ± 0.1	–	16.5 ± 0.2	16.6 ± 0.2	–	–	0.38 ± 0.19
21	20.9 ± 0.0	21.0 ± 0.0	19.9 ± 0.1	19.5 ± 0.0	19.2 ± 0.0	18.9 ± 0.0	19.2 ± 0.2	15.9 ± 0.0	15.9 ± 0.0	13.9 ± 0.0	11.7 ± 0.0	5.84 ± 0.18
22	–	–	–	–	20.6 ± 0.2	20.7 ± 0.3	–	16.7 ± 0.1	16.6 ± 0.1	–	13.8 ± 0.1	0.96 ± 0.18
23	24.4 ± 0.0	–	–	–	21.1 ± 0.2	20.7 ± 0.2	19.5 ± 0.3	15.7 ± 0.0	14.9 ± 0.0	14.2 ± 0.0	13.1 ± 0.0	0.86 ± 0.16
24	21.5 ± 0.0	21.4 ± 0.1	20.9 ± 0.2	19.5 ± 0.0	19.2 ± 0.1	19.0 ± 0.1	19.1 ± 0.2	16.8 ± 0.1	16.7 ± 0.1	15.7 ± 0.2	13.6 ± 0.1	0.83 ± 0.17

3. SED Plots

Analyzing Spectral Energy Distributions helped to categorize the clumps into two main groups, those with evidence of recent active star formation, or starbursts, and those with a more quiescent profile indicative of an older stellar population. A starburst profile shows excess emission in the UV and mid-infrared, while a quiescent distribution has an approximately blackbody curve from the combined light of the stars, smoothly sloping up from lower UV values, peaking in the optical, and then smoothly sloping down to the infrared. The excess emission in starburst profiles is above this blackbody curve. The excess in the 5.8 and 8.0 μm wavelengths originates from interstellar grains and molecules heated mainly by young stars. Excess emission in the UV is from recently formed hot stars.

Examples of starburst and quiescent profiles can be seen in Figure 2. Clump 4 is an example of a starburst SED and clump 12 is an example of a quiescent SED. Clump 4 is located in the southern arc of Arp 107, while clump 12 is outside the ring, east of the primary galaxy. From this analysis it appears that most of the clumps have active star formation, with clumps 4, 5, 6, 7, 8, 10, 11, 15, 16, 17, 18, 20, 21, 22, 24, 26, and 29 having SEDs of starbursts, while clumps 1, 2, 3, 9, 12, 13, 14, 25, 27, and 28 show distributions that are quiescent. Clump 23 has an odd spectrum with an excess of infrared emission, possibly indicating a background quasar. This is consistent with color-color plots in Smith et al. (2005) that place clump 23 with typical data for quasars. Clump 9 has a spectrum indicative of a foreground star, and its redshift shows it is not part of Arp 107 (Keel, private communication in Smith et al. 2005). Both the nucleus of the companion (clump 28) and the nucleus of the primary galaxy (clump 14) have SED profiles indicating an older stellar population. The SED plots for each clump can be found in the Appendix.

Table 1—Continued

ID	FUV	NUV	u	g	r	i	z	3.6 μm	4.5 μm	5.8 μm	8.0 μm	Hα
25	23.4 ± 0.0	–	–	21.4 ± 0.2	20.0 ± 0.1	19.3 ± 0.1	18.9 ± 0.2	15.8 ± 0.0	15.7 ± 0.0	–	15.6 ± 0.3	0.17 ± 0.16
26	20.4 ± 0.0	20.2 ± 0.0	19.6 ± 0.1	19.2 ± 0.0	19.0 ± 0.0	18.9 ± 0.1	18.9 ± 0.2	15.4 ± 0.0	15.5 ± 0.0	13.4 ± 0.0	11.3 ± 0.0	9.17 ± 0.17
27	21.8 ± 0.0	21.5 ± 0.0	–	19.8 ± 0.1	19.0 ± 0.0	18.7 ± 0.0	19.0 ± 0.2	16.0 ± 0.1	15.7 ± 0.1	15.3 ± 0.1	14.2 ± 0.1	–
28	21.9 ± 0.0	21.0 ± 0.0	17.7 ± 0.0	15.9 ± 0.0	15.0 ± 0.0	14.6 ± 0.0	14.3 ± 0.0	11.8 ± 0.0	11.9 ± 0.0	11.8 ± 0.0	11.6 ± 0.008	–
29	21.3 ± 0.0	21.1 ± 0.0	20.4 ± 0.2	19.6 ± 0.0	19.3 ± 0.0	19.1 ± 0.1	19.2 ± 0.2	16.5 ± 0.1	16.6 ± 0.1	16.2 ± 0.3	13.8 ± 0.1	0.81 ± 0.16
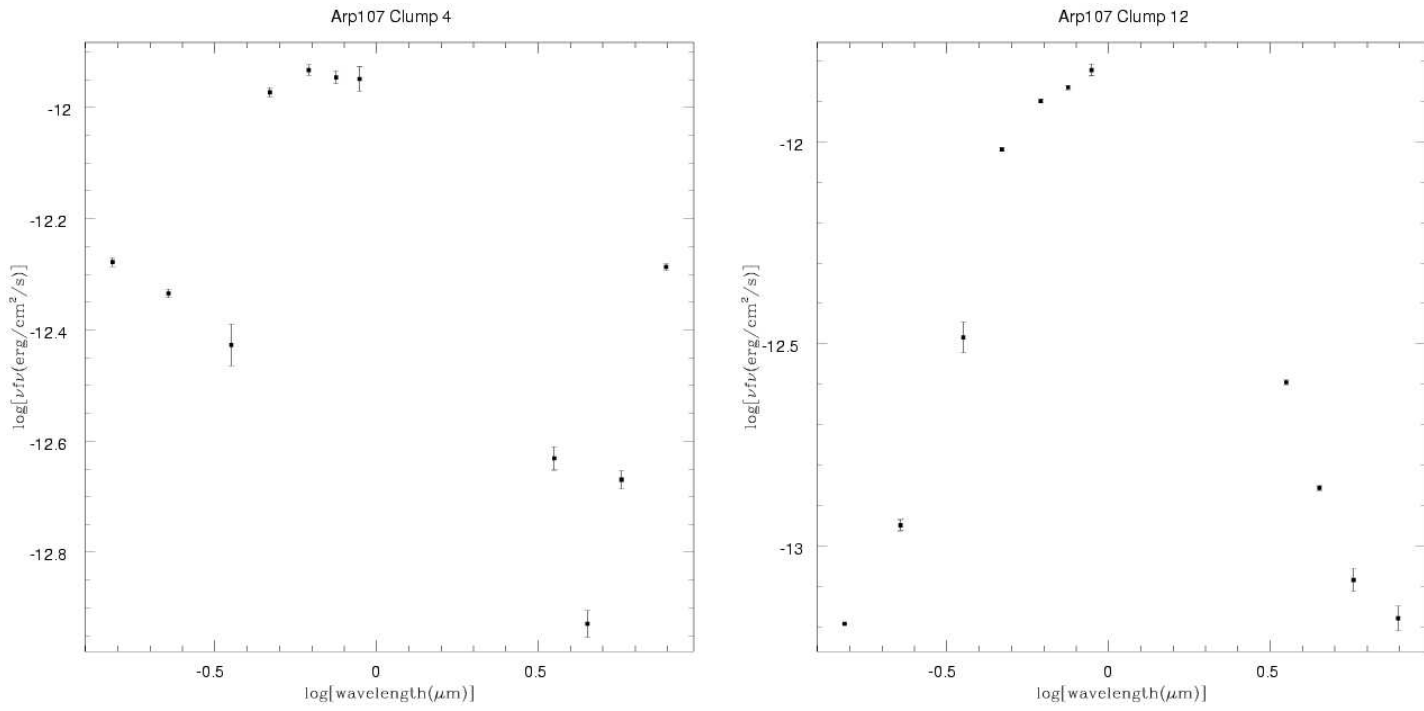
Fig. 2.— Clump 4 has a Spectral Energy Distribution indicative of starbursts, while clump 12 has a distribution indicative of quiescent star formation

4. Color-Color Plots

To determine various properties of the regions we made color-color plots of different wavelengths and compared to results of Spitzer colors found in Smith et al. (2005). Figure 3 displays the [3.6]-[8.0] vs. NUV-g and [3.6]-[8.0] vs. g-r plots. The nucleus of the companion, clump 28, has the lowest [3.6]-[8.0] color (close to zero), and is very red in the [NUV]-[g] band, thus it is probably very old with little active star formation. The primary nucleus, clump 14, has a [3.6]-[8.0] color of more than 2, and is bluer than clump 28 in the [NUV]-[g] band, so it is not as old as the companion nucleus and may still have some star formation. Clump 12 has a low [3.6]-[8.0] color, as well as a quiescent SED profile, so it may be a background/foreground star. The [g]-[r] colors indicate a very old stellar age for clump 9, reaffirming that it is a foreground star. Other clumps that appear to have older stellar populations are 25, 3, 11, 28, 14, 27, 2 and 12. However this band is affected by extinction so some colors may be misleading.

5. Position Angle vs. Color-Color

A sequence in the age of the star forming regions can be inferred from plotting the different color-color magnitudes as a function of position angle. A trend in the [4.5]-[5.8] color was recognized in Smith et al. (2005) as a possible sequence in stellar ages around the spiral arm. This trend is shown in Figure 4 along with several different colors plotted against position angle to further investigate the possibility of a sequence in ages among the clumps. The clump colors in the [3.6]-[8.0] bands decrease from the northern tip clockwise along the galaxy, starting with clumps 26 and 21 with colors greater than 4, followed by clumps 10 and 16, then 4, 5, and 7, with 6 and 8 just below. This implies a sequence in the mass-normalized star formation rate along the primary galaxy arm. The NUV-g and g-r magnitudes have similar patterns. Clump 17 is more red than clump 15, and from there
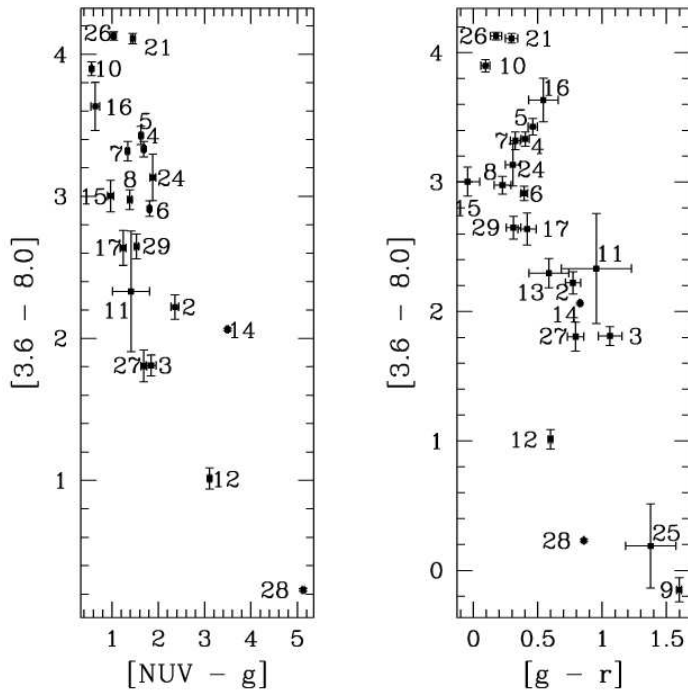
Fig. 3.— Color-color plots for [3.6]-[8.0] vs. NUV-g and [3.6]-[8.0] vs. g-r.

the clumps get more red until peaking around 6, 4 and 5, then decrease to clump 7 and finally clump 10. In the FUV-NUV band the increasing pattern is still evident, but is not as well defined. However there is a decreasing sequence from clump 16 to clump 21. These patterns suggest a sequence in the age of the clumps around the arm of the galaxy, with clumps in the northern part of the galaxy younger than clumps in the southern part of the galaxy. The FUV-NUV band is also a measure of extinction so it could be that the galaxy has more extinction in the east and south and less in the west and north.

6. Population Synthesis Modeling

To determine the ages and extinctions of the clumps we superimposed population synthesis models used in Smith et al. (2008) on various color-color plots. An example of the superimposed plots used is shown in Figure 5. The remaining plots can be found in the Appendix. The population synthesis models were made using Starburst99 version 5.1 (Leitherer et al. 1999) and include the Padova asymptotic giant-branch stellar models (Vazquez & Leitherer 2005). These models assume an instantaneous burst with a Kroupa initial mass function. The model ages start at an age of 1 Myr, then increase by 1 Myr steps to 20 Myr, then by 5 Myr steps to 50 Myr, then 10 Myr steps to 100 Myr, 100 Myr steps to 1 Gyr, and 500 Myr steps to 10 Gyr. Three sets of models are shown, with extinctions of E(B-V) equal to 0, 0.5 and 1. The colors used were FUV-NUV, NUV-g, u-g, g-r, r-i, and i-z. We ran a script written by Mark Hancock to compute the ages and extinctions using a chi squared minimization calculation (Hancock et al. 2009). The results are in Table 2 along with the colors used in the fits. Only detections were used to calculate the ages; upper limits were ignored.

Plotting these results as a function of position angle gives evidence of a sequence of increasing age along the spiral arm in clumps 21, 16, 10, 7, 5, 4, 6, 8, and 15, as seen in
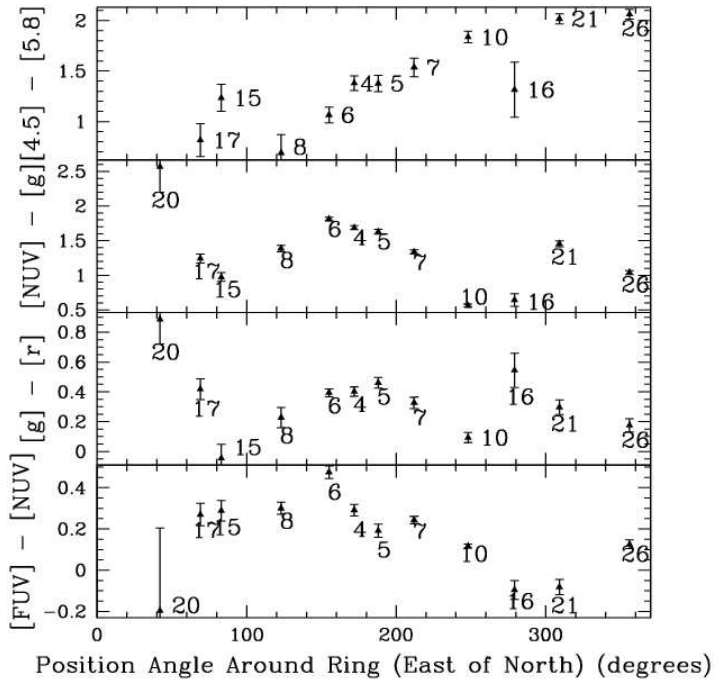
Fig. 4.— Different colors for clumps in the spiral arm as a function of position angle.

Figure 6. The extinction is highest for clumps in the southern tip of the galaxy with E(B-V) roughly 0.2. It is not as prevalent in the eastern and western parts of the galaxy, but seems to affect clumps in the northern part of the galaxy similarly.

By comparing the ages of clumps at the base of the tail (East) to those around the middle of the tail (South) and the end of the tail (West), an estimation for the star formation propagation rate can be made. The three areas in question (base/middle/end) are each separated by about 100 degrees along the arc. With a radius of 20 kpc this gives a distance of about 35 kpc from base to middle and from middle to end. If we associate an age of around 100 Myrs to the base (clumps 15 and 8), 40 Myrs for the middle clumps (4 and 5), and 10 Myrs at the end (clumps 16 and 21), we get a base/middle star formation propagation rate of 0.58 kpc/Myr (567 km/s) and a middle/end star formation propagation rate of 1.2 kpc/Myr (1173 km/s).

These values were then compared to the simulation of the interaction presented in Smith et al. (2005). If we isolate a few frames in the model where star formation seems to be most active in the base, middle, and tail of the arc and calculate a star formation propagation rate from the model time, it is much lower (more than a factor of 10) than the star formation propagation rate calculated from the Starburst99 results. In the model star formation does not move smoothly along the arm, but occurs in random locations of stochastic star formation. A comparison can also be made to the models presented by Wallin (1990), who investigates density compression along tidal features. In their Figure 3, they show density vs. time for various locations along a tidal feature in a prograde planar interaction. The density enhancement moves from the base of the tail to near the end in about 0.85 model time units, a distance of about 1 model unit. In his scale, this converts to roughly 0.21 kpc/Myr (205 km/s), 3-6 times smaller than the rate we infer for the Arp 107 tail from the Starburst99 models.

Another discrepancy between the model and observations is the amount of star formation in the companion nucleus. The spectral energy distribution of the companion nucleus is indicative of a very old stellar population with little recent star formation, however, the model predicts a large amount of active star formation in the companion nucleus. This could be due to the model parameters being more favorable for accretion from the primary galaxy compared to the actual system. Another possibility is that the model companion initially had too much gas, meaning it should be an earlier-type galaxy.

In the future, the Starburst99 fitting could be changed for better results by using two initial stellar populations (old and young), or having more than one burst of star formation. As seen in Table 2, for some clumps the reduced chi square is significantly larger than 1. This implies a poor fit, which may indicate a second age component in the clump.

7.   Additional Plots

Additional plots were created to observe various trends between star formation indicators. In Figure 7 the FUV luminosity is plotted against Hα luminosity and a positive correlation was observed as expected, since both of these bands trace recent star formation. Clump 10 show the largest FUV luminosity, while clump 14 shows the largest Hα luminosity. Clump 26 has the next highest values, followed by 4, 5, and 7 grouped with slightly more FUV and 16 and 21 with more Hα. Below 4, 5, and 7 are 6, 8, 15 and 17, and below 16 and 21 are 29 and 24. Clump 2 is isolated with the least amount of Hα luminosity, and clumps 13, 18, 20 and 25 all have significantly lower values than the main group. FUV luminosity is also plotted against the 8.0 micron luminosity in figure 8, and a similar trend is once again observed because both variables are tracers of recent star formation. At 8.0 microns clump 14 stands out as the highest value, and clump 10 likewise in the FUV. Clump 26 is next, followed by clumps 4 and 5. Clump 21 is nearby but with slightly less FUV luminosity, and

Table 2.   Population Synthesis Results

ID	Age (Myr)	Extinction E(B-V)	Reduced χ Squared	Colors Used
1	$1\pm^2_0$	$0.12\pm^{0.52}_{0.12}$	0.165	FUV-NUV
2	$8\pm^1_1$	$0.56\pm^{0.06}_{0.06}$	38.222	FUV-NUV, NUV-g, g-r, r-i, i-z
3	$9\pm^2_1$	$0.56\pm^{0.08}_{0.06}$	32.566	FUV-NUV, NUV-g, g-r, r-i, i-z
4	$40\pm^{34}_8$	$0.3\pm^{0.06}_{0.1}$	85.064	FUV-NUV, NUV-g, u-g, g-r, r-i, i-z
5	$37\pm^7_{32}$	$0.3\pm^{0.16}_{0.04}$	65.273	FUV-NUV, NUV-g, u-g, g-r, r-i, i-z
6	$113\pm^{21}_{27}$	$0.18\pm^{0.06}_{0.04}$	124.267	FUV-NUV, NUV-g, u-g, g-r, r-i, i-z
7	$35\pm^{10}_8$	$0.24\pm^{0.06}_{0.06}$	81.152	FUV-NUV, NUV-g, u-g, g-r, r-i, i-z
8	$94\pm^{35}_{30}$	$0.1\pm^{0.06}_{0.06}$	21.108	FUV-NUV, NUV-g, u-g, g-r, r-i, i-z
9	$8\pm^1_1$	$1.18\pm^{0.02}_{0.04}$	1066.218	g-r, r-i, i-z
10	$27\pm^6_6$	$0.1\pm^{0.04}_{0.04}$	10.940	FUV-NUV, NUV-g, u-g, g-r, r-i, i-z
11	$9\pm^{23}_2$	$0.44\pm^{0.22}_{0.22}$	7.610	FUV-NUV, NUV-g, g-r, r-i, i-z
12	$125\pm^{175}_{18}$	$0.5\pm^{0.04}_{0.18}$	327.284	FUV-NUV, NUV-g, u-g, g-r, r-i, i-z
14	$7\pm^1_1$	$0.84\pm^{0.02}_{0.02}$	609.720	FUV-NUV, NUV-g, u-g, g-r, r-i, i-z
15	$102\pm^{24}_{58}$	$0\pm^{0.12}_0$	11.409	FUV-NUV, NUV-g, u-g, g-r, r-i, i-z
16	$9\pm^2_2$	$0.22\pm^{0.06}_{0.1}$	12.905	FUV-NUV, NUV-g, u-g, g-r, r-i
17	$32\pm^{15}_{21}$	$0.24\pm^{0.1}_{0.08}$	22.142	FUV-NUV, NUV-g, u-g, g-r, r-i, i-z
20	$5\pm^2_2$	$0.76\pm^{0.2}_{0.18}$	1.912	FUV-NUV, NUV-g, g-r, r-i
21	$13\pm^2_7$	$0.34\pm^{0.04}_{0.08}$	38.293	FUV-NUV, NUV-g, u-g, g-r, r-i, i-z
22	$4\pm^{2996}_3$	$0.9\pm^{1.12}_{0.9}$	–	r-i
23	$4\pm^{10096}_3$	$2\pm^{0.02}_{1.72}$	2.108	r-i, i-z
24	$7\pm^{84}_1$	$0.4\pm^{0.06}_{0.2}$	8.340	FUV-NUV, NUV-g, u-g, g-r, r-i, i-z
26	$32\pm^{10}_{27}$	$0.18\pm^{0.12}_{0.06}$	4.677	FUV-NUV, NUV-g, u-g, g-r, r-i, i-z
27	$10\pm^2_3$	$0.48\pm^{0.06}_{0.08}$	38.292	FUV-NUV, NUV-g, g-r, r-i, i-z
29	$35\pm^{14}_{30}$	$0.28\pm^{0.14}_{0.08}$	4.414	FUV-NUV, NUV-g, u-g, g-r, r-i, i-z
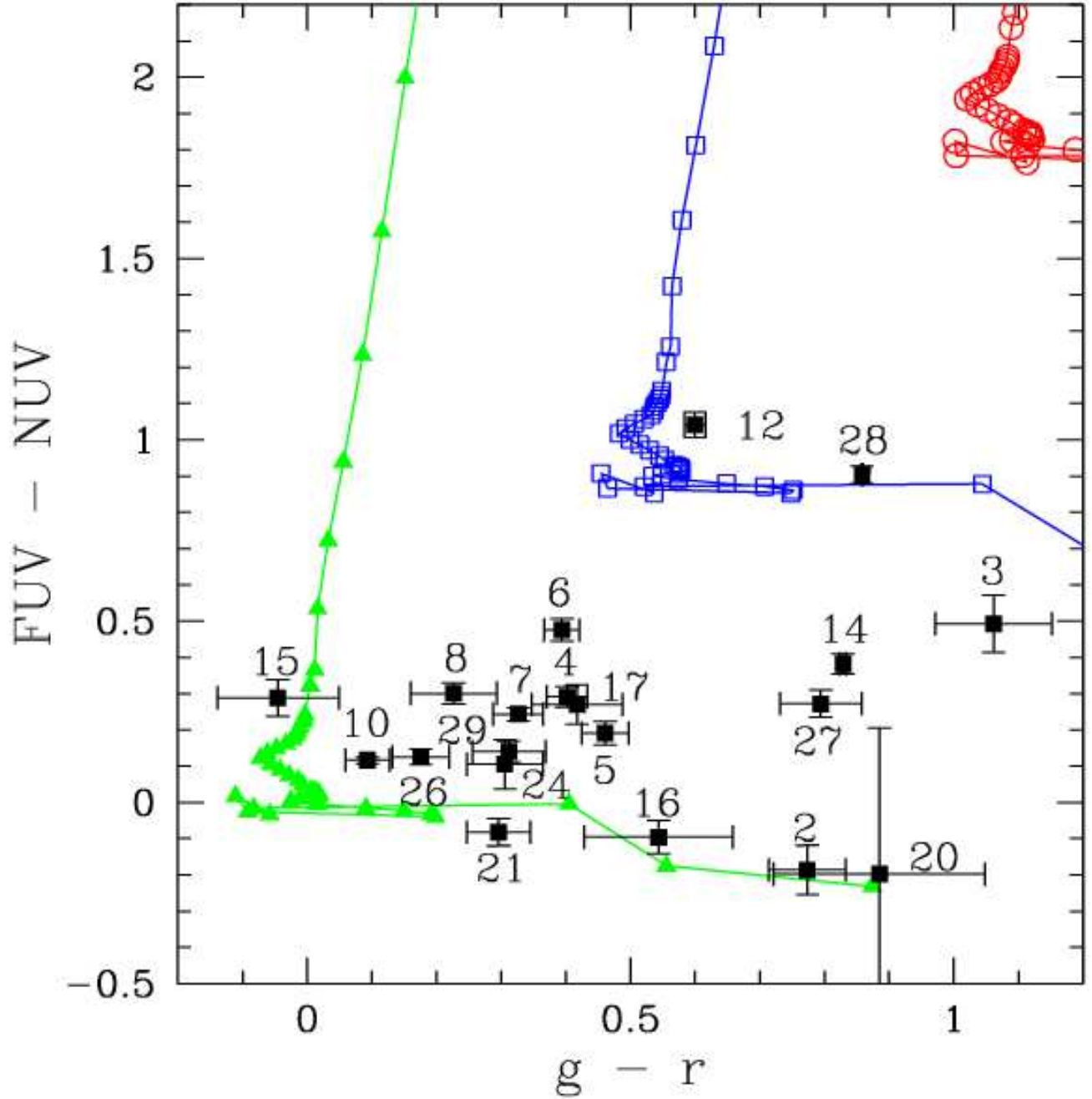
Fig. 5.— The green triangles show the population synthesis model with E(B-V) = 0, the blue squares show E(B-V) = 0.5, and the red squares show E(B-V) = 1.0. The model ages start at an age of 1 Myr, then increase by 1 Myr steps to 20 Myr, then by 5 Myr steps to 50 Myr, then 10 Myr steps to 100 Myr, 100 Myr steps to 1 Gyr, and 500 Myr steps to 10 Gyr. The clumps from Arp 107 are labeled as in Figure 1.

clumps 6 and 7 are close too, but with less 8.0 micron luminosity. Clump 28 shows a very low FUV luminosity. As in the SED plot, this is likely an older stellar population with few young stars. The remaining clumps follow almost perfectly in line except for 23, which is probably a background quasar. In order of decreasing amounts of recent star formation, the remaining clumps are 8, 15, 17, 16, 24, 29, 27, 11, 2, 12, 3, 13, 19, 1, 18 and 25.

Spitzer colors [3.6]-[8.0] were plotted against 8.0 micron luminosity in figure 9 and again a positive trend is observed as expected. The [3.6]-[8.0] color is a measure of the mass normalized star formation rate, and 8.0 micron luminosity traces recent star formation, so regions of primarily older stars with less active star formation are in the bottom left, while regions of mostly new stars with active star formation are in the upper right. Clumps 26, 21, and 10 are the some of the youngest clumps with recent star formation. Clump 16 is shortly behind them in [3.6]-[8.0] magnitude, but has a much lower 8.0 micron luminosity, meaning it may not have much active star formation. Clumps 4, 5, and 7 are the next group of fairly young clumps, accompanied by clump 6, which is close but probably contains a slightly older population since it has a lower [3.6]-[8.0] magnitude. Clump 9 has the lowest age, another indication that it is just a foreground star. The companion nucleus (clump 28) shows a largely older stellar population with a [3.6]-[8.0] magnitude of 0.2, but still has a large amount recent star formation. The main nucleus (clump 14) has the highest 8.0 micron luminosity of any clump, probably due to dust heating by the Seyfert nucleus. Clump 25 is far below any other clump, so it has very little star formation or any young stars. In figure 10 the [3.6]-[8.0] color is also plotted against $2.5\log(H\alpha)$-r, a measure of the $H\alpha$ equivalent width. There is a clear increasing trend among the clumps, with clumps 21, 26 and 10 at the top right, followed by 16, then 4, 5, and 7 and down through 24, 15, 8, 6, 22, 29, 17, 23, 13, and 2. Clumps 14 and 25 are not grouped with the others for various reasons. Clump 14 has an $H\alpha$ equivalent width much greater than any other due to its Seyfert nucleus. Clump 25 shows little to no signs of star formation and an old stellar

population.

Both the 8.0 micron and the FUV wavelengths are tracers of star formation, but the FUV is affected by extinction, unlike the 8.0 micron, thus the [8.0]-FUV color is a measure of extinction, and is plotted against 8.0 micron luminosity in figure 11. As the 8.0 micron luminosity values increase, the [8.0]-FUV values decrease, so clumps with more recent star formation show more extinction. Clumps 1, 3, 12, 13, and 19 show more extinction for their amount of star formation as compared to the general trend. Clumps 18 and 25 are slightly removed from the main group as well with very little recent star formation or extinction. To further examine extinction FUV-[8.0] is plotted against FUV-NUV magnitudes in figure 12. A strong trend is observed as expected. The companion nucleus (clump 28) is reddest in FUV - [8.0], with clump 14 (the main nucleus) close by. The FUV-NUV magnitudes were also plotted against the absolute magnitude in the optical r band in figure 13. The SDSS color u-g is plotted against $2.5\log(H\alpha)$-r in figure 14. Clump 14, the primary nucleus, has a higher $H\alpha$ equivalent width than any other clump due to its Seyfert nucleus. Clumps 21, 26, and 10 are grouped together with the next highest equivalent width values, followed by 4, 5, and 7. Clumps 6 and 16 appear to have larger values than the remaining clumps, but the uncertainty on these clumps is large. The u-g band is a rough estimate of age but is highly affected by extinction. Using this to order the clumps by decreasing age results in 8, 14, 4, 6, 7, 24, 5, 17, 15, 29, 10, 21, 26 and 16.

8. Conclusions

In Smith et al. (2005) a strong azimuthal variation in the [4.5] - [5.8] colors of clumps was seen in the ring/primary arm of Arp 107, implying a variation in the ratio of the number of old stars to the number of young stars. In the current paper, this relation was investigated further with UV and optical imaging, and population synthesis modeling was

done to estimate the ages of the star forming clumps in Arp 107. The ages found showed a pattern of an older population (around 100 Myrs old) at the base of the arm that transitions into a younger population (around 10 Myrs old) near the tip, however, the star formation propagation rate calculated from these estimates does not agree with propagation rates found in other papers, namely Wallin (1990). This may be due to the existence of two main populations of stars, both a young population and an older underlying stellar population.

9. Appendix

In the Appendix we present SED plots for the individual clumps. These are displayed in figures 15-22. We also provide an additional population synthesis models superimposed over clump magnitudes in figures 23-26.
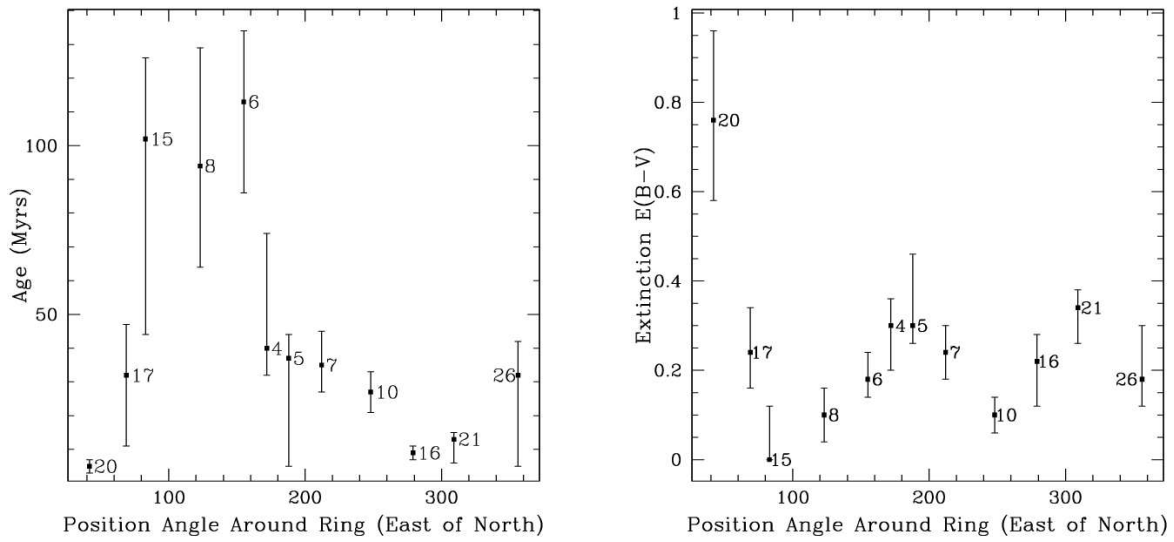
Fig. 6.— Plotting age as a function of position angle makes the increasing sequence around the spiral arm clear. Knowing the extinctions as well allows a clearer interpretation.
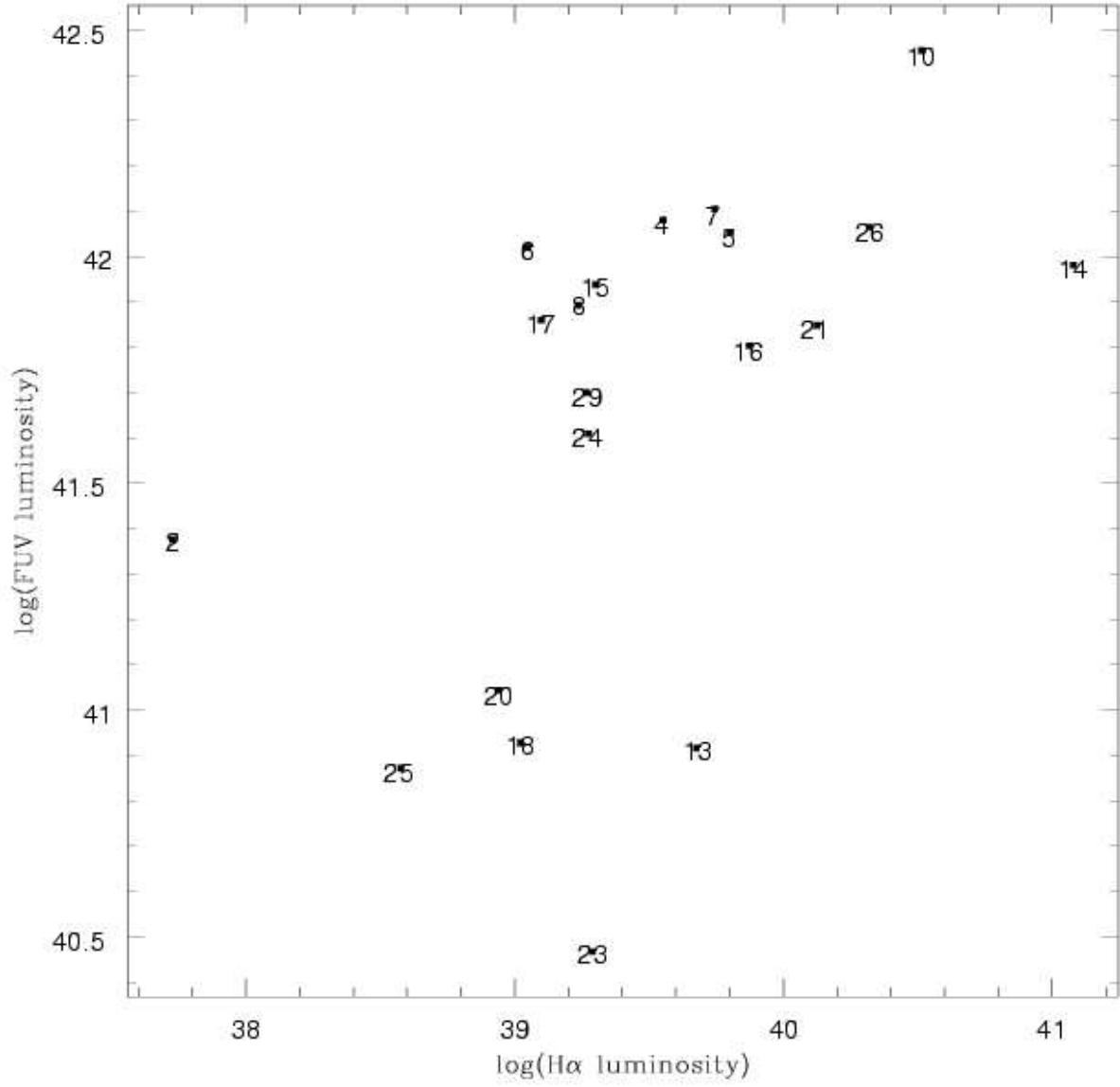
Fig. 7.— A log-log plot of FUV luminosity vs. Hα luminosity for the clumps identified in Figure 1.
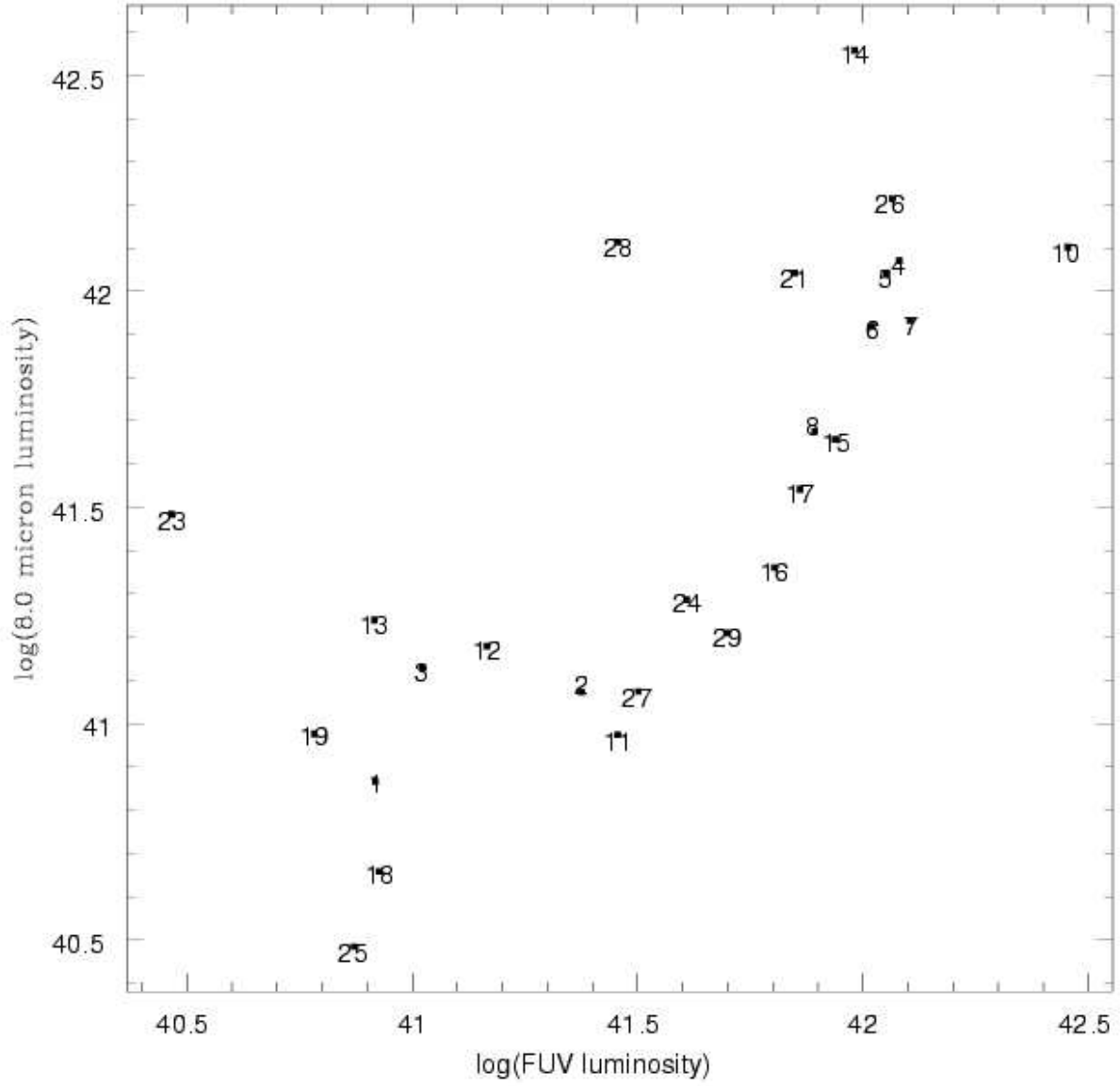
Fig. 8.— A log-log plot of 8.0 micron luminosity vs. FUV luminosity for the clumps identified in Figure 1.
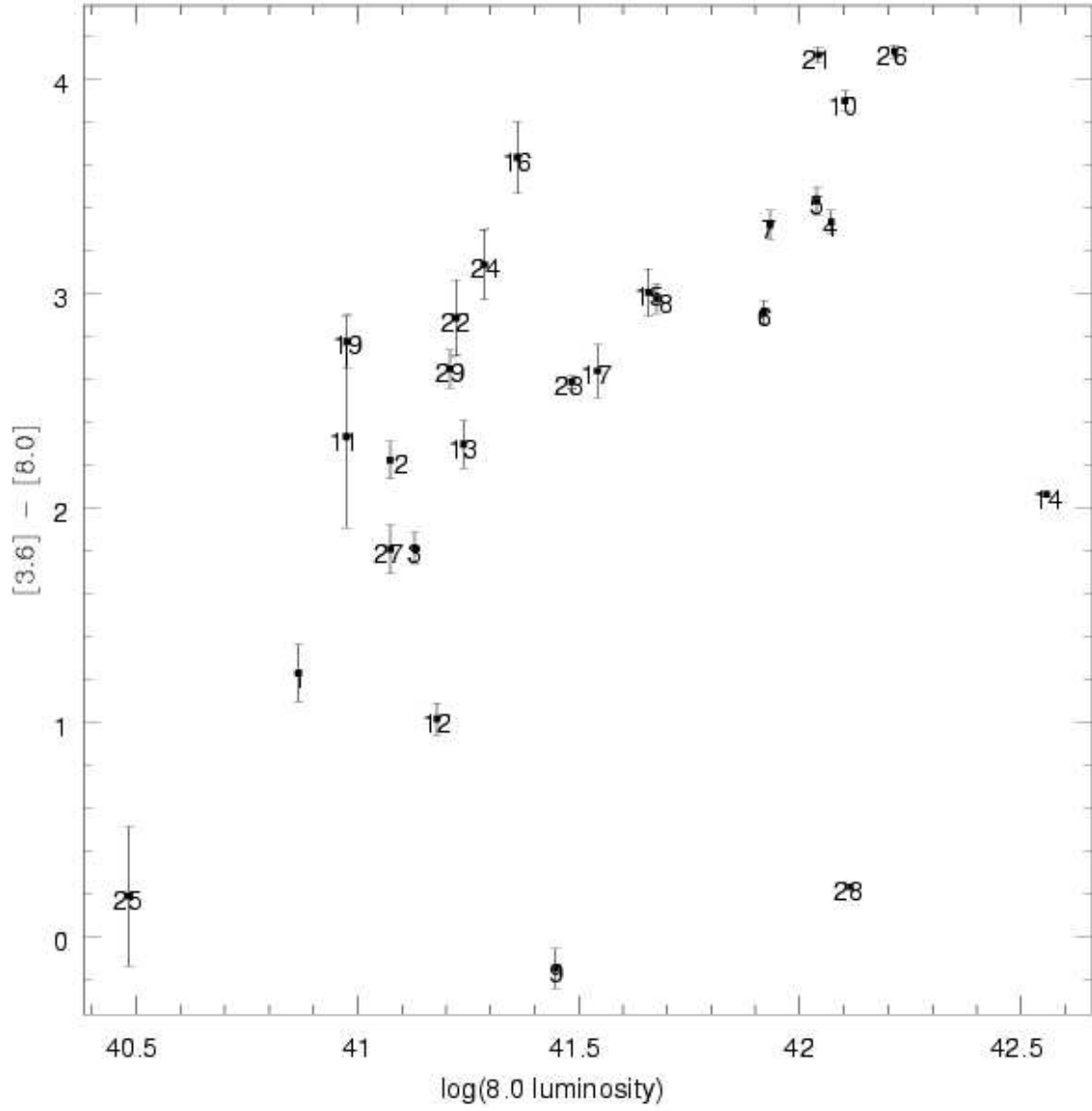
Fig. 9.— The [3.6] - [8.0] color is plotted against the logarithm of the 8.0 micron luminosity for the clumps identified in Figure 1.
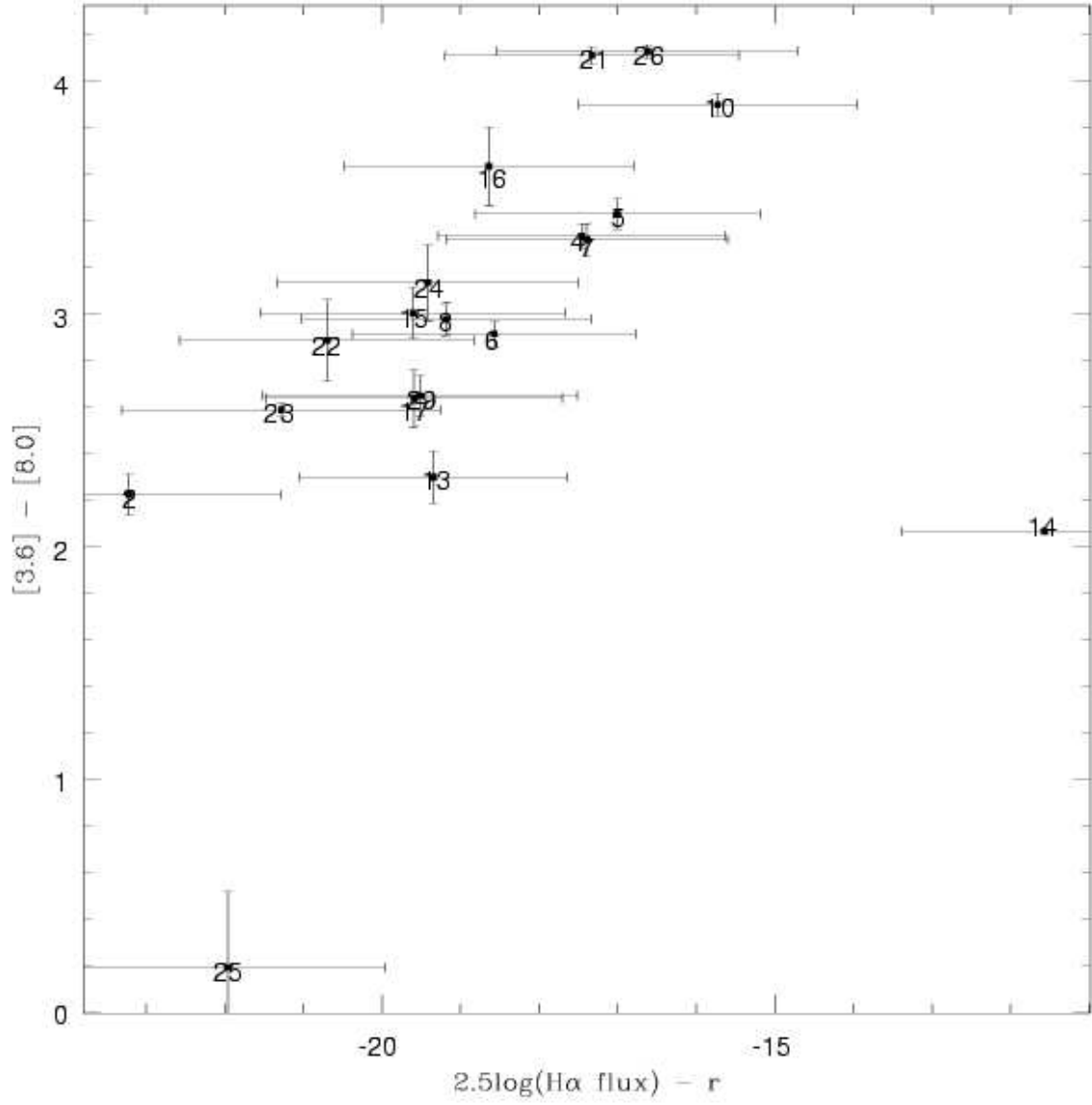
Fig. 10.— The [3.6] - [8.0] color is plotted against Hα equivalent width for the clumps identified in Figure 1.
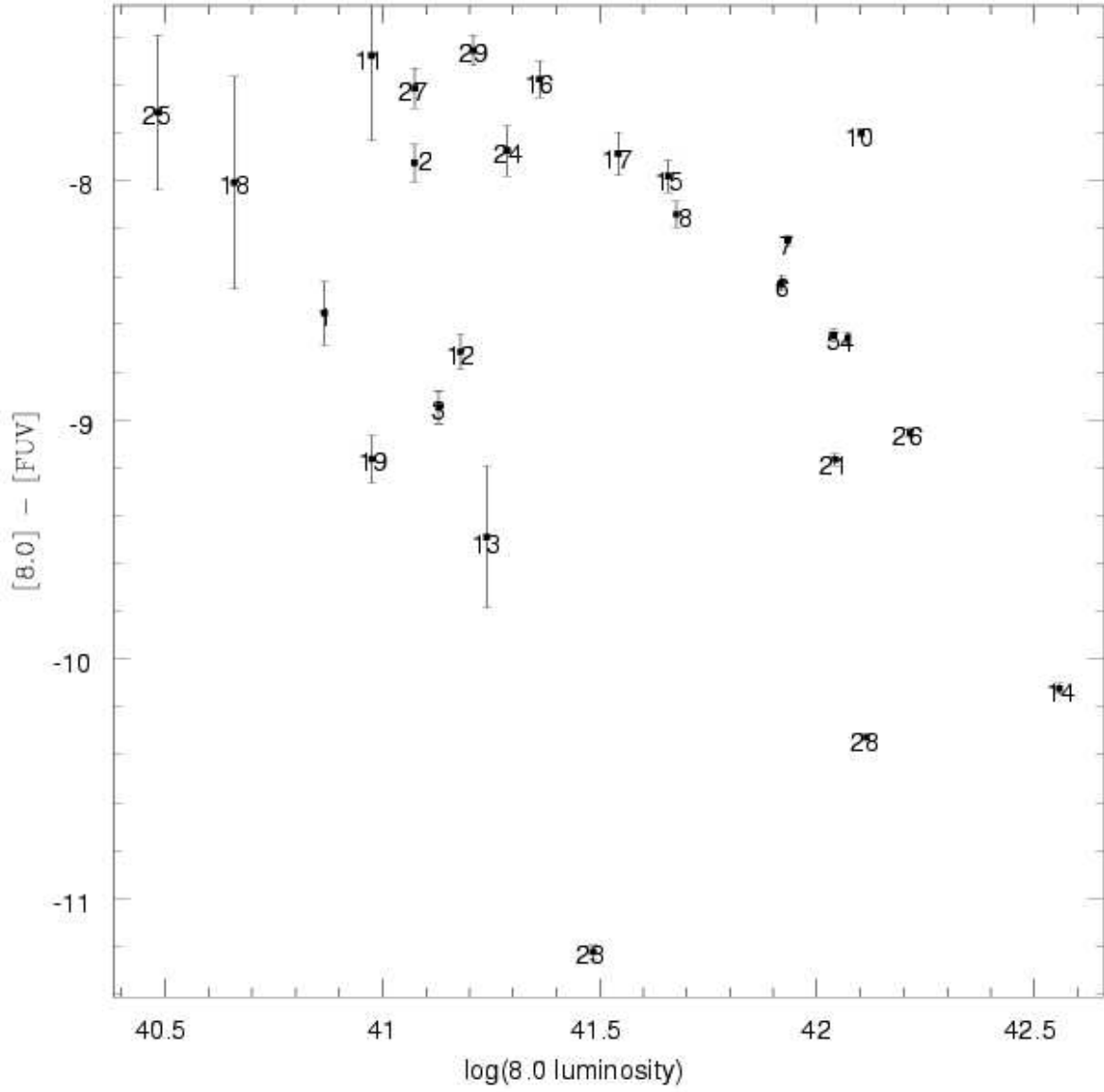
Fig. 11.— The [8.0] - FUV color is plotted against the logarithm of the 8.0 micron luminosity for the clumps identified in Figure 1.
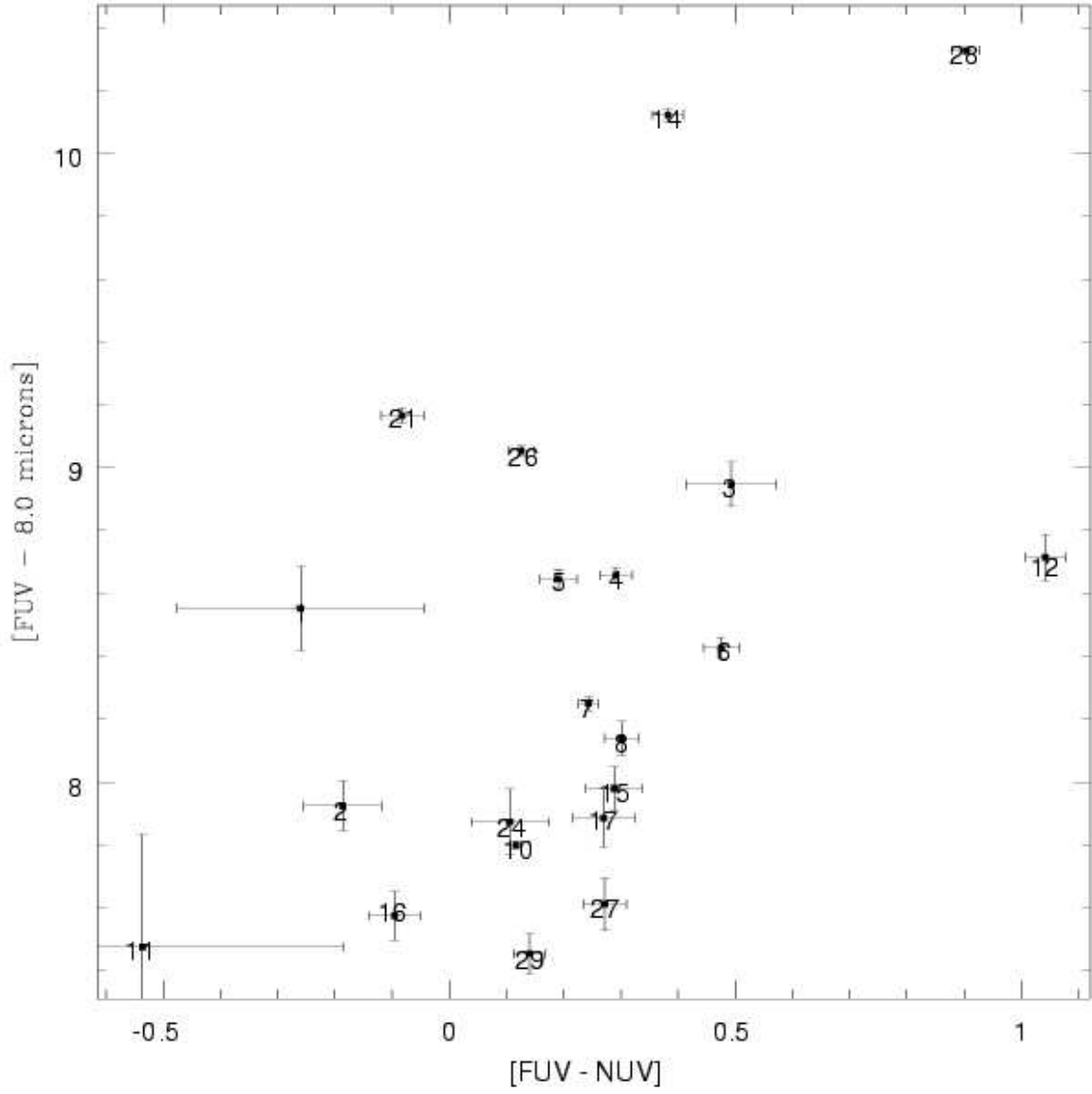
Fig. 12.— A color - color plot of FUV - [8.0] vs. FUV - NUV for the clumps identified in Figure 1.
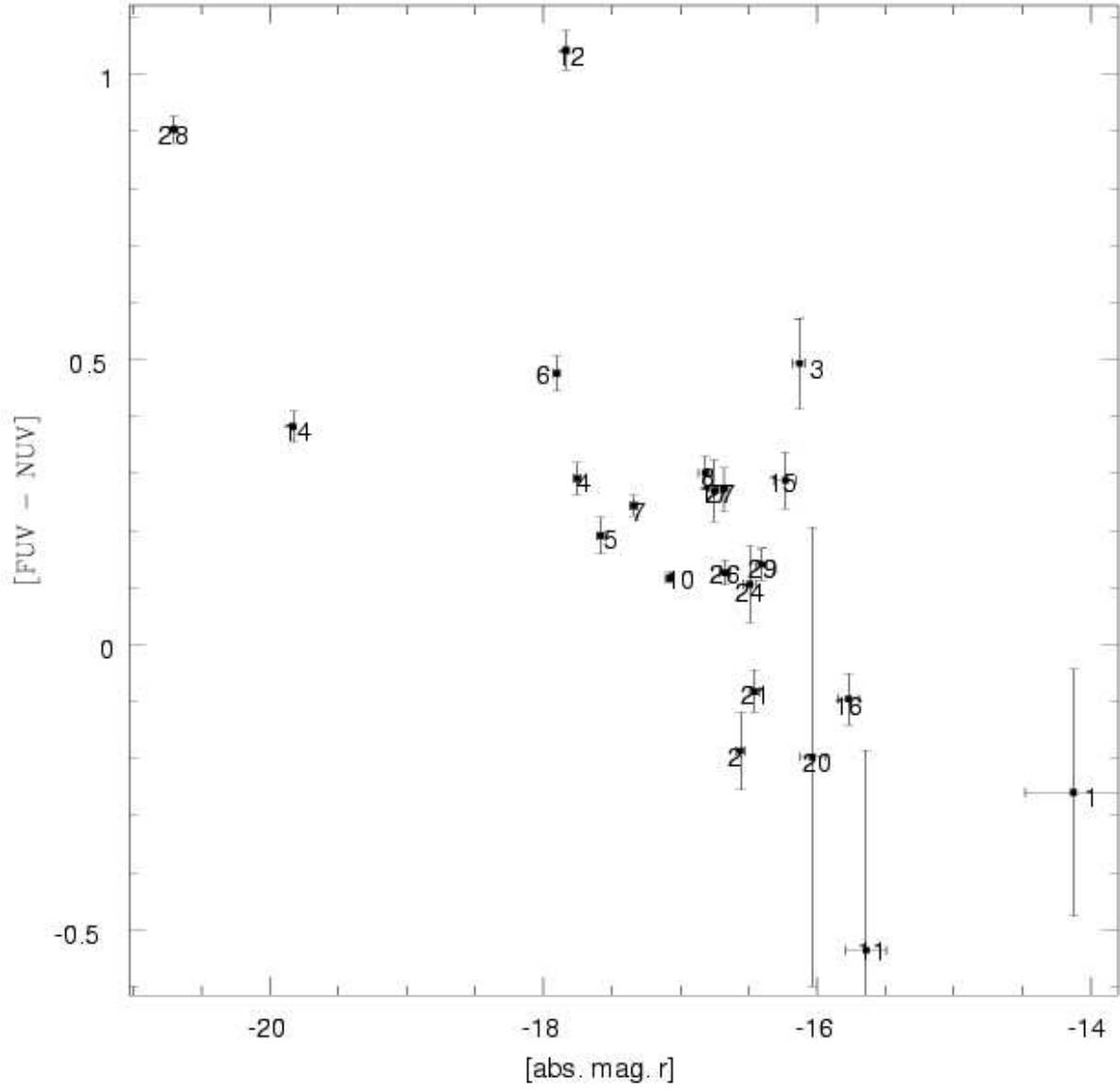
Fig. 13.— The FUV - NUV color is plotted against the absolute magnitude of the r band for the clumps identified in Figure 1.
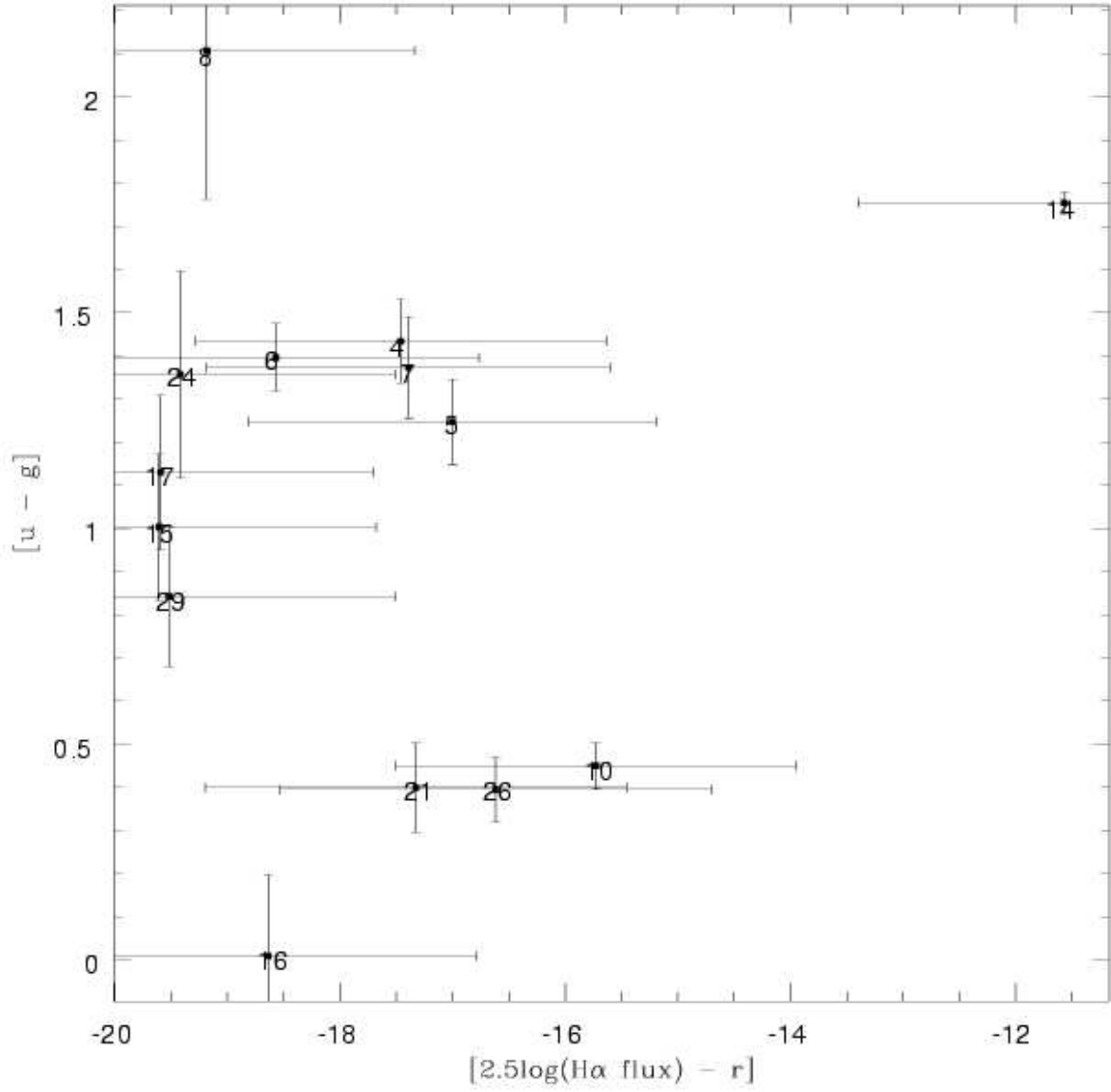
Fig. 14.— The u - g color is plotted against the Hα equivalent width for the clumps identified in Figure 1.
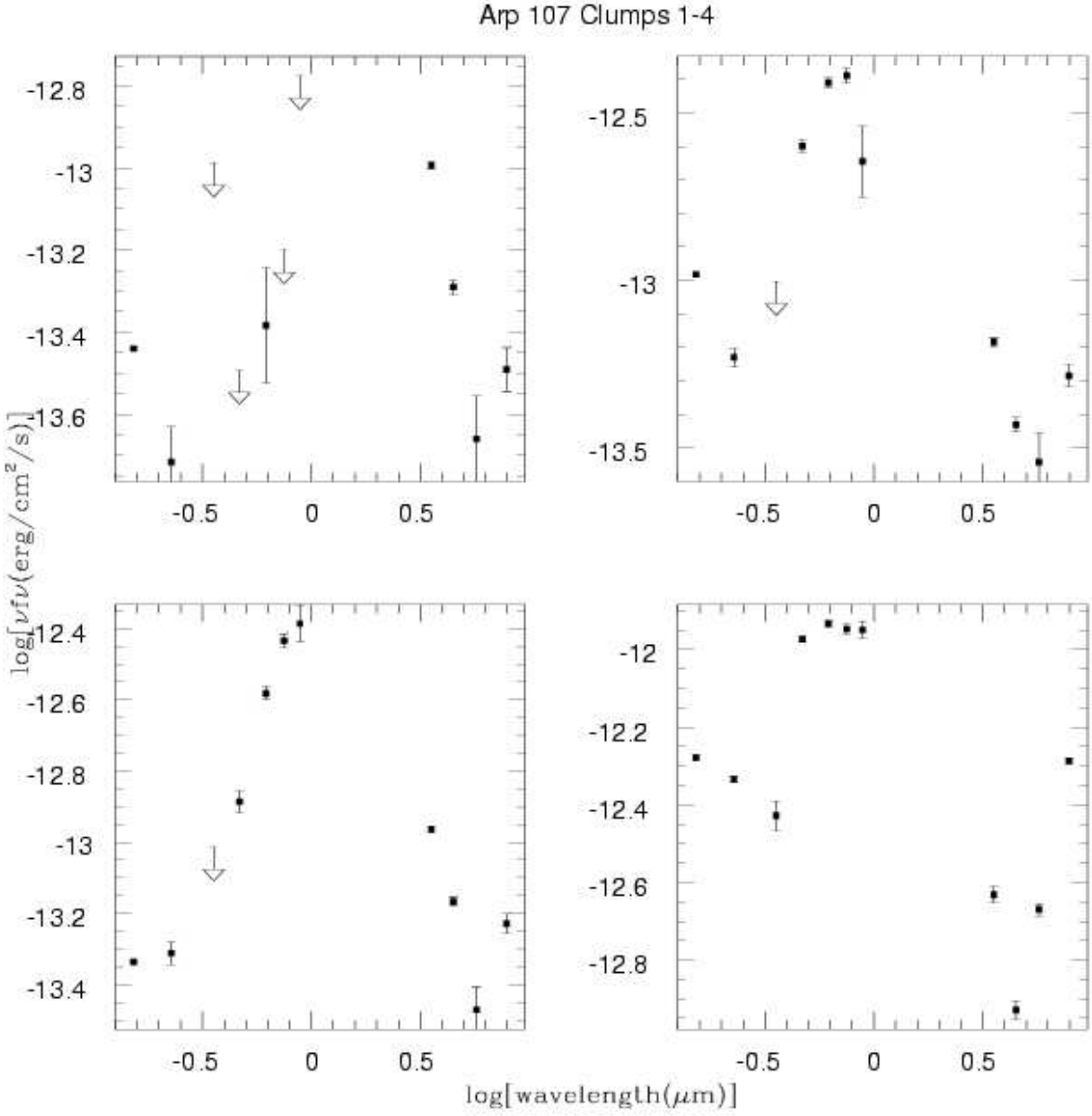
Fig. 15.— SED plots of clumps 1-4. Downward pointing arrows indicate an upper limit.
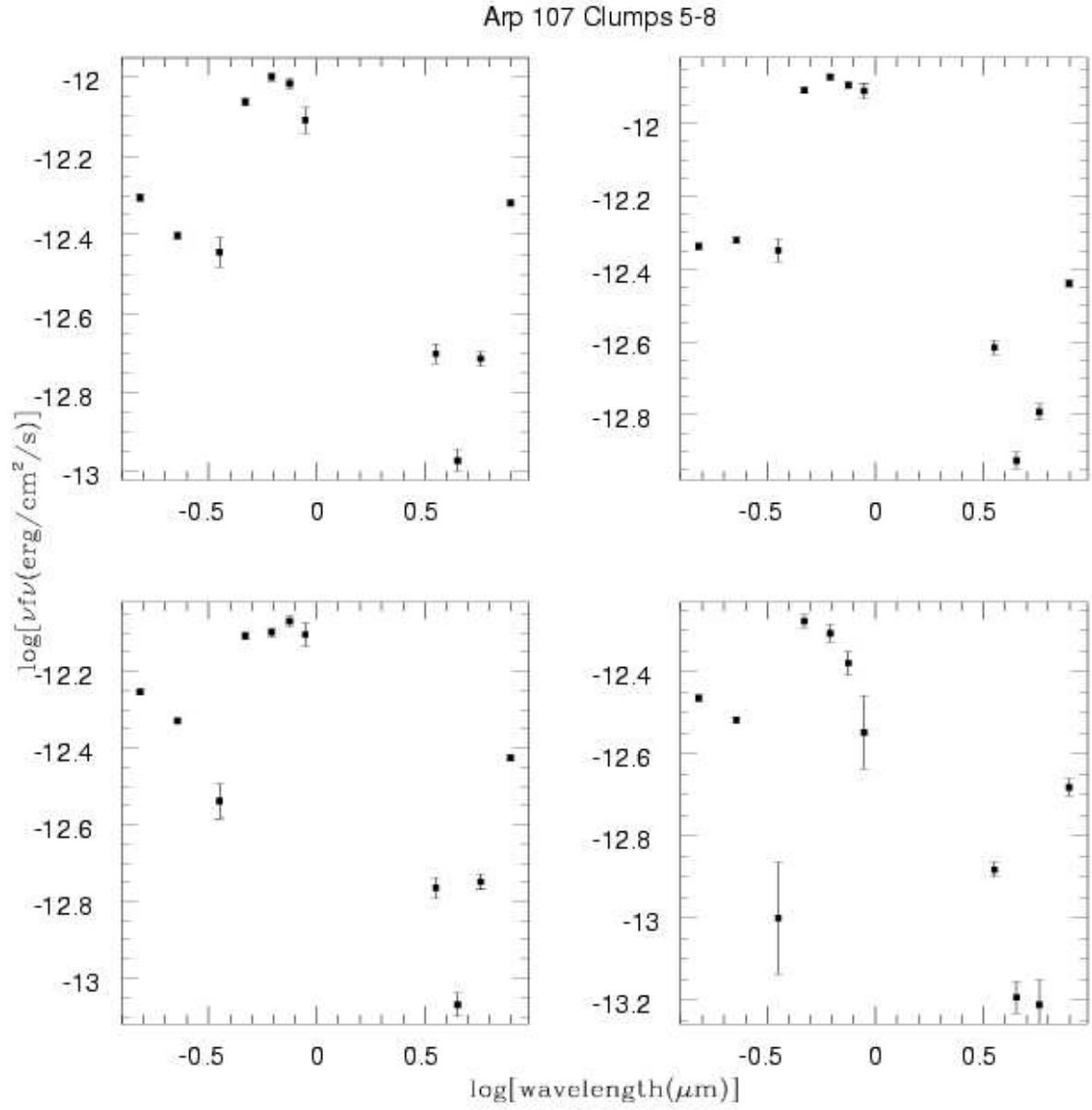
Fig. 16.— SED plots of clumps 5-8. Downward pointing arrows indicate an upper limit.
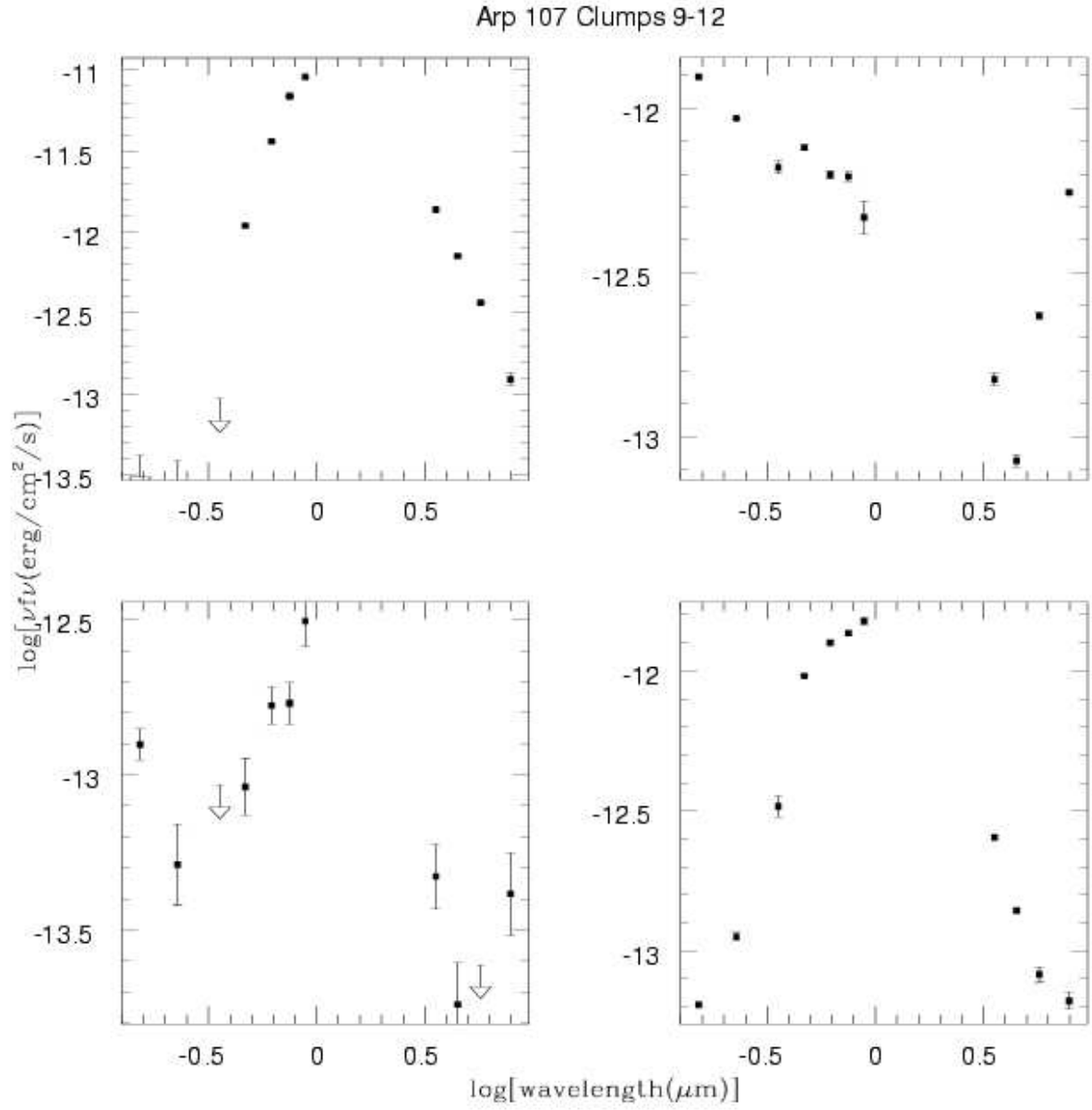
Fig. 17.— SED plots of clumps 9-12. Downward pointing arrows indicate an upper limit.
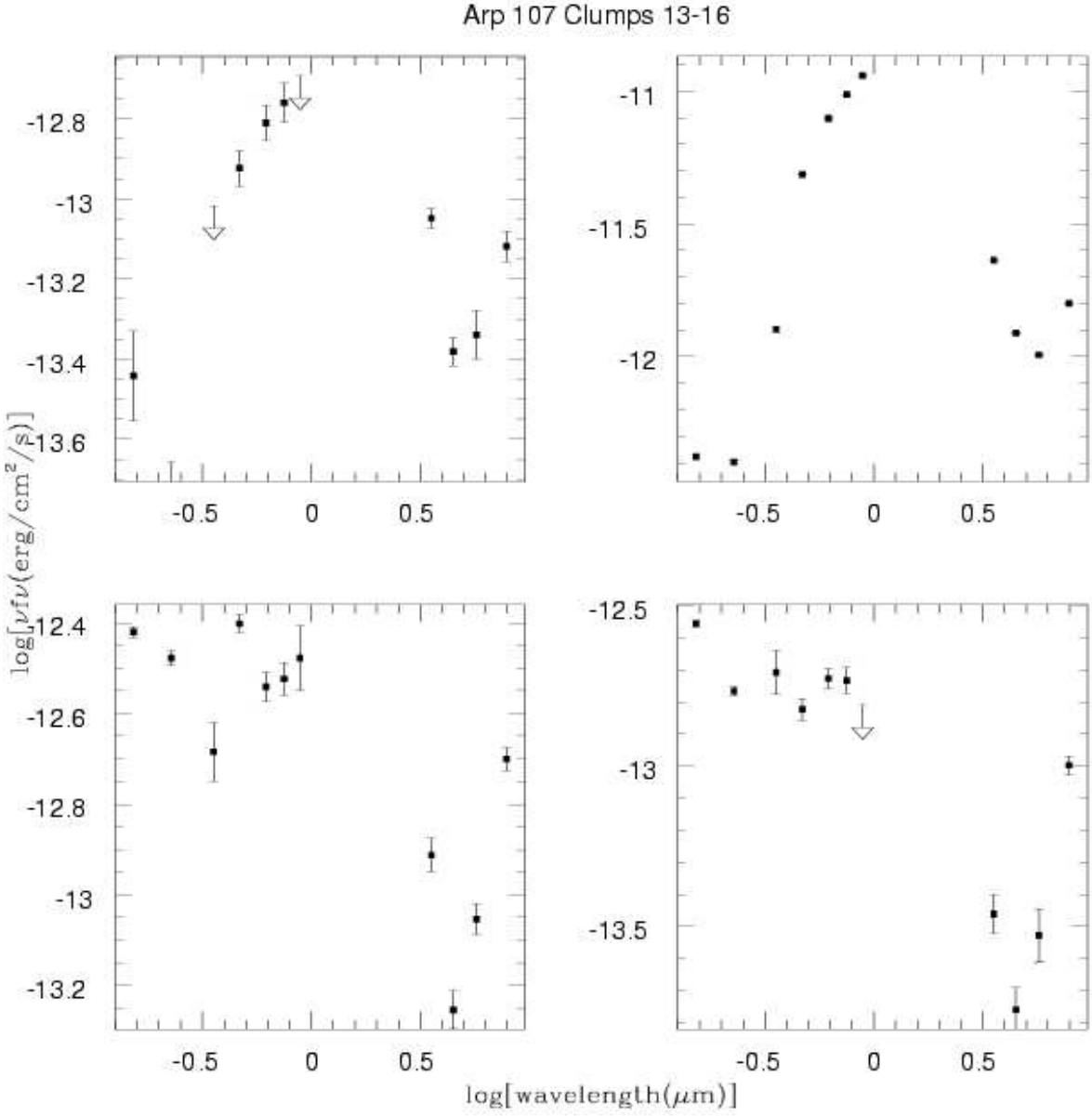
Fig. 18.— SED plots of clumps 13-16. Downward pointing arrows indicate an upper limit.
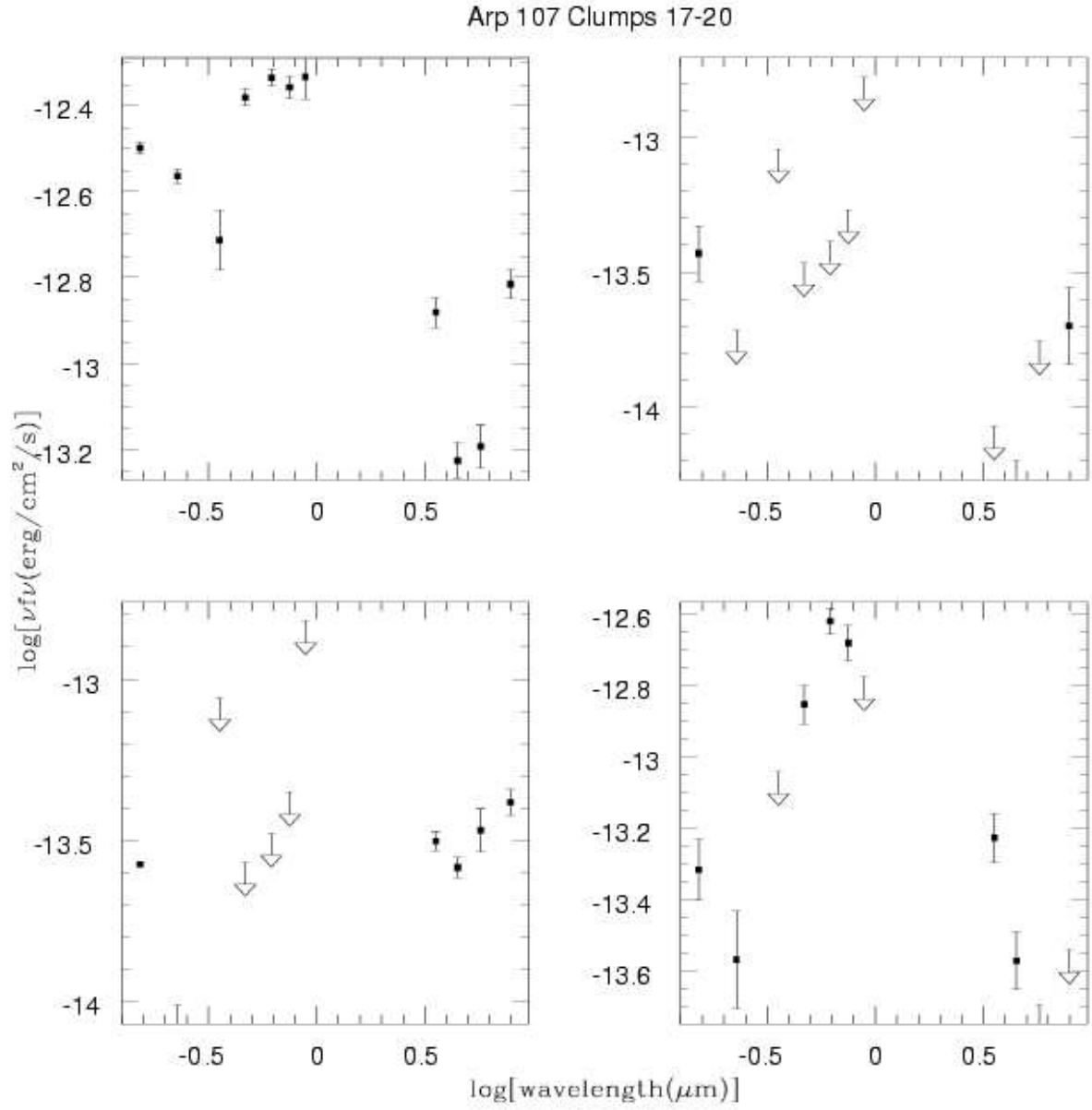
Fig. 19.— SED plots of clumps 17-20. Downward pointing arrows indicate an upper limit.
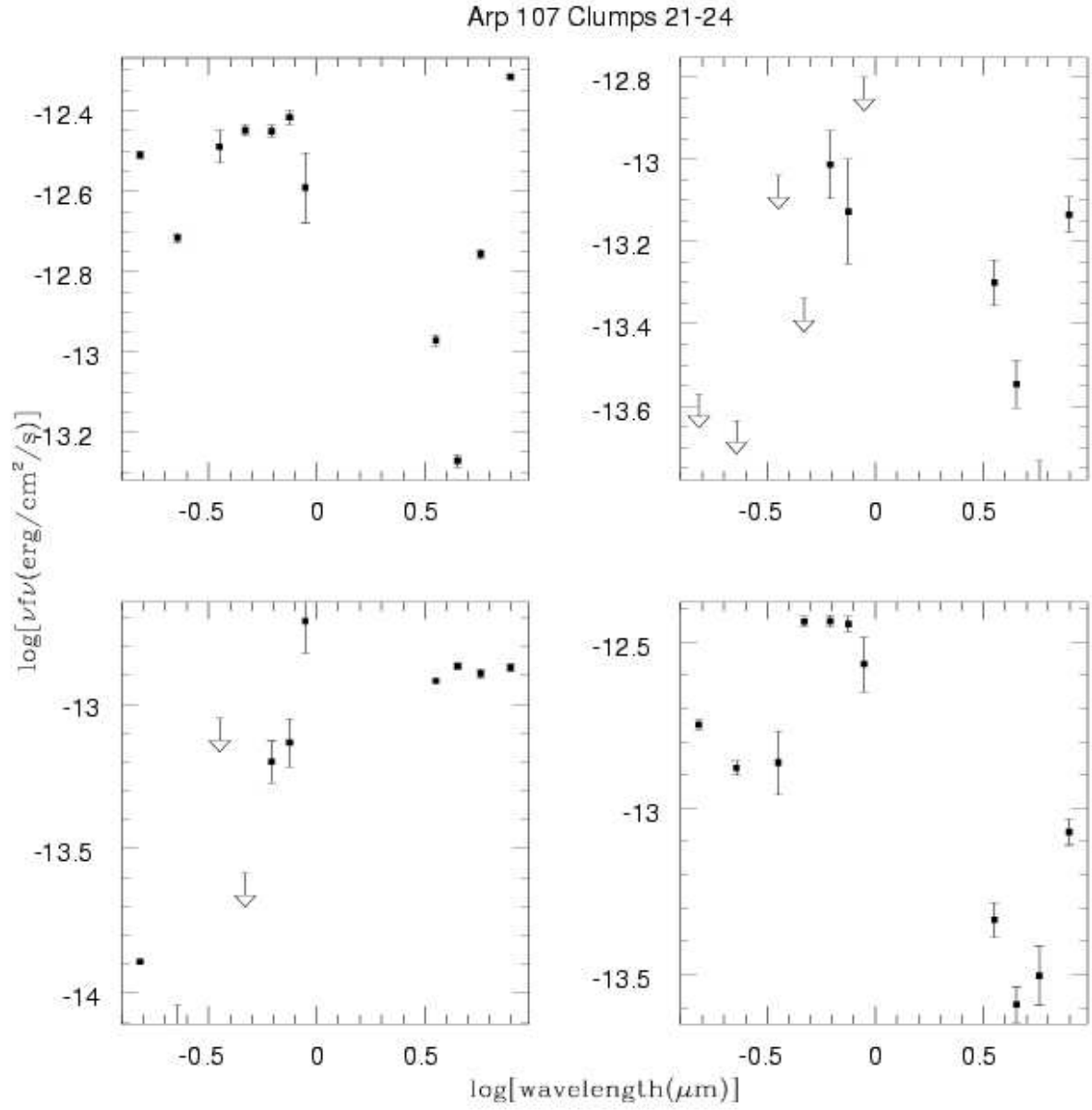
Fig. 20.— SED plots of clumps 21-24. Downward pointing arrows indicate an upper limit.
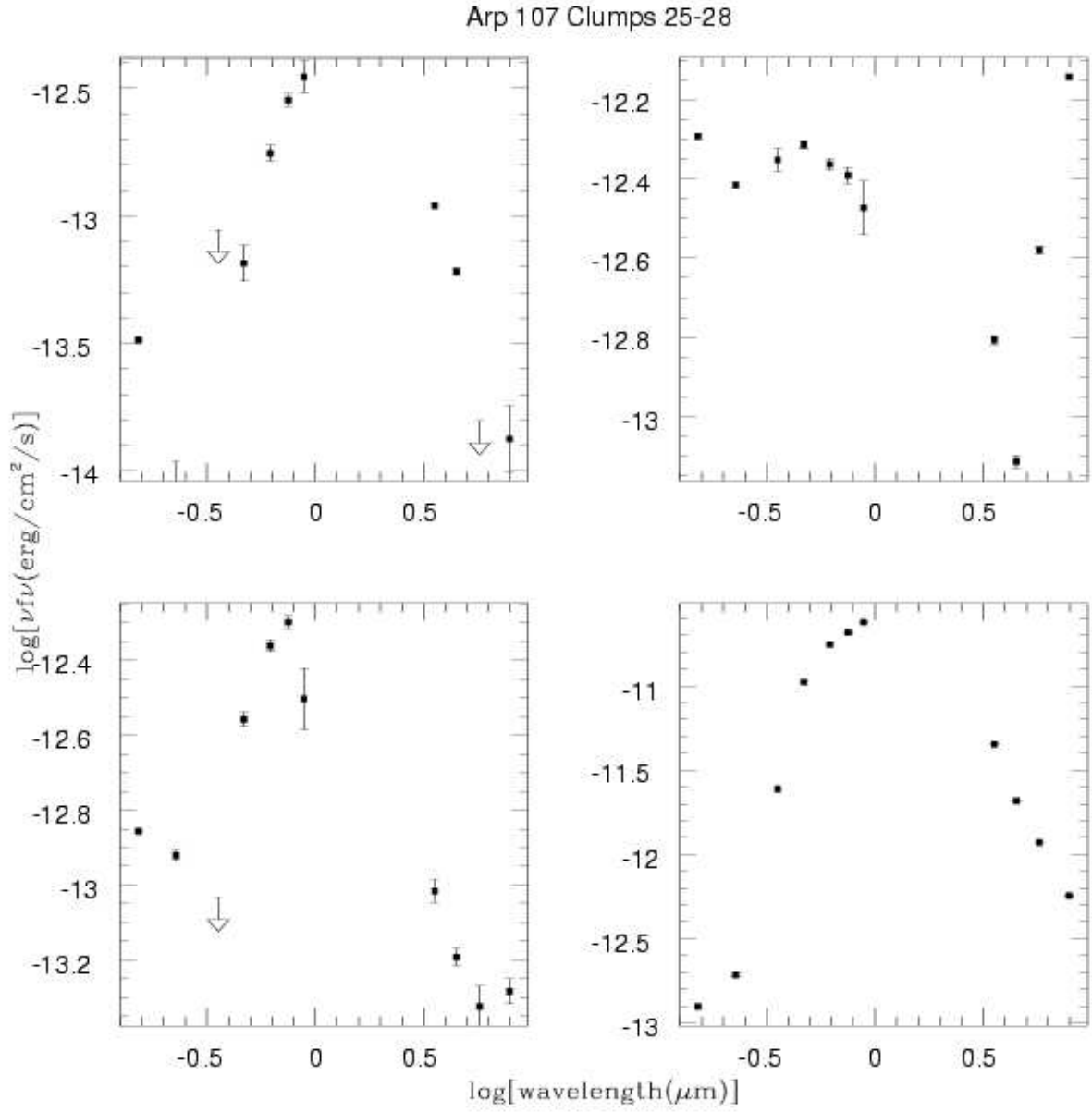
Fig. 21.— SED plots of clumps 25-28. Downward pointing arrows indicate an upper limit.
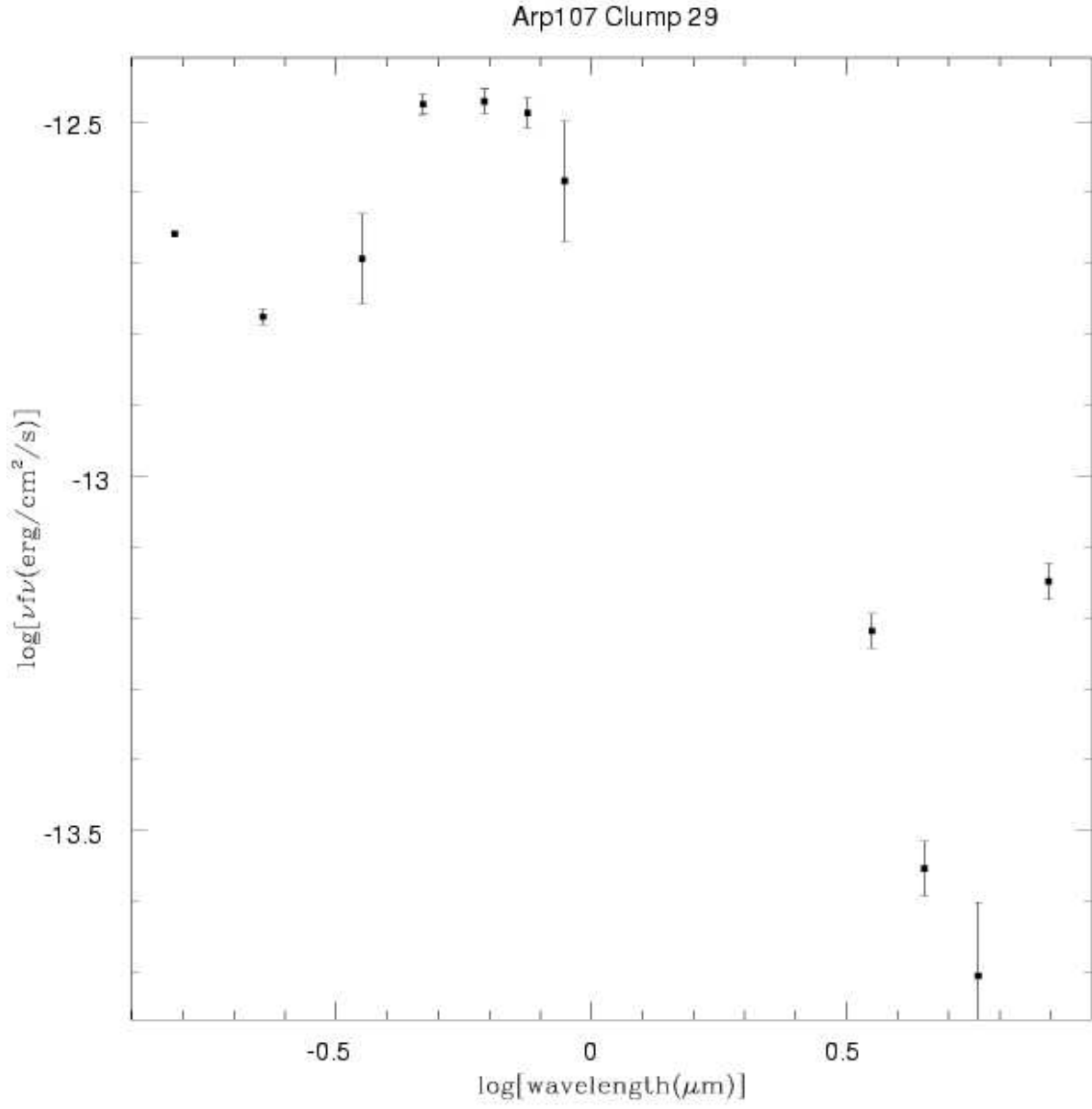
Fig. 22.— SED plot of clump 29. Downward pointing arrows indicate an upper limit.
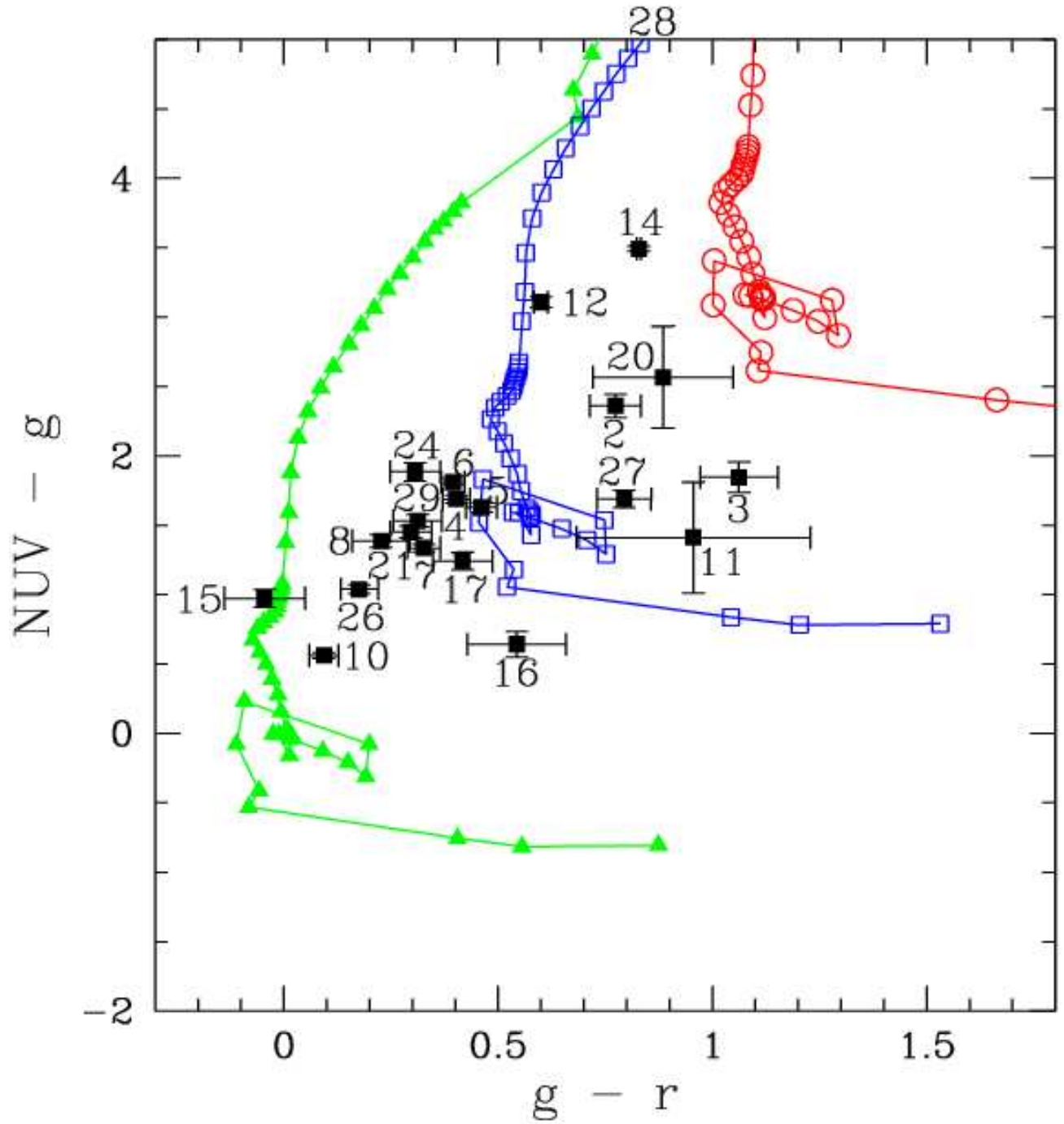
Fig. 23.— The green triangles show the population synthesis model with E(B-V) = 0, the blue squares show E(B-V) = 0.5, and the red squares show E(B-V) = 1.0. The model ages start at an age of 1 Myr, then increase by 1 Myr steps to 20 Myr, then by 5 Myr steps to 50 Myr, then 10 Myr steps to 100 Myr, 100 Myr steps to 1 Gyr, and 500 Myr steps to 10 Gyr. The clumps from Arp 107 are labeled as in Figure 1.
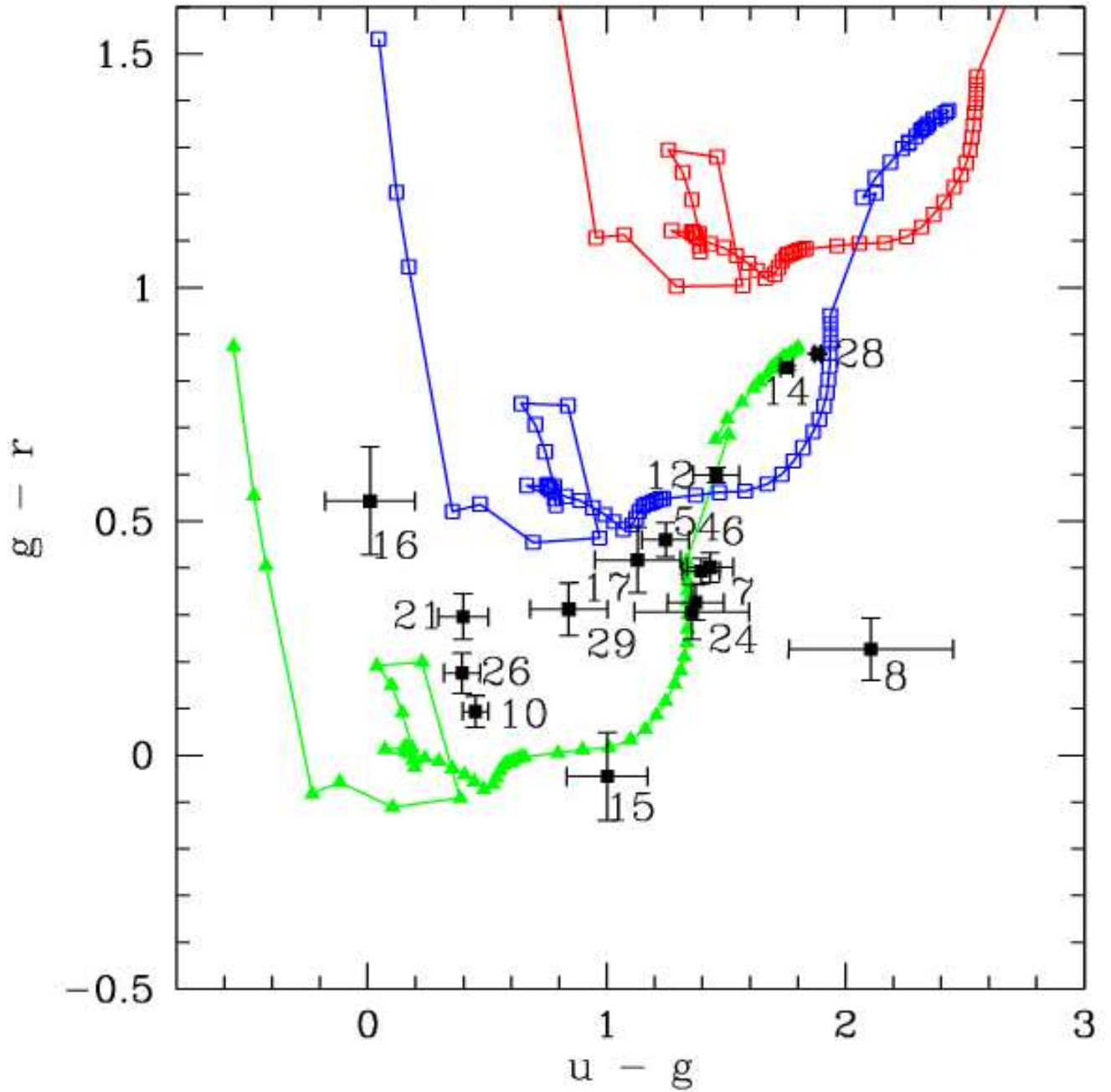
Fig. 24.— The green triangles show the population synthesis model with E(B-V) = 0, the blue squares show E(B-V) = 0.5, and the red squares show E(B-V) = 1.0. The model ages start at an age of 1 Myr, then increase by 1 Myr steps to 20 Myr, then by 5 Myr steps to 50 Myr, then 10 Myr steps to 100 Myr, 100 Myr steps to 1 Gyr, and 500 Myr steps to 10 Gyr. The clumps from Arp 107 are labeled as in Figure 1.
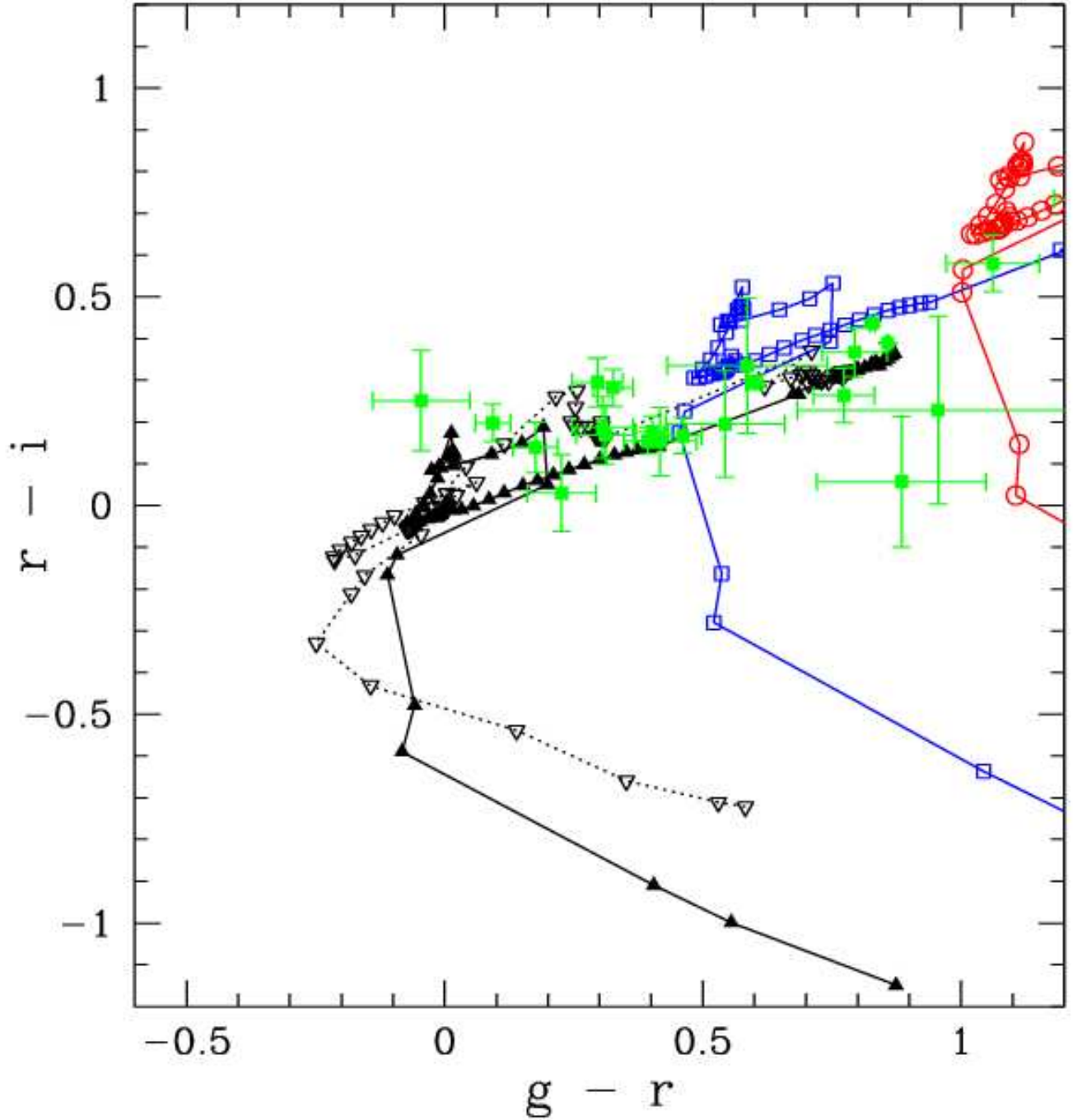
Fig. 25.— The green triangles show the population synthesis model with E(B-V) = 0, the blue squares show E(B-V) = 0.5, and the red squares show E(B-V) = 1.0. The model ages start at an age of 1 Myr, then increase by 1 Myr steps to 20 Myr, then by 5 Myr steps to 50 Myr, then 10 Myr steps to 100 Myr, 100 Myr steps to 1 Gyr, and 500 Myr steps to 10 Gyr. The clumps from Arp 107 are labeled as in Figure 1.
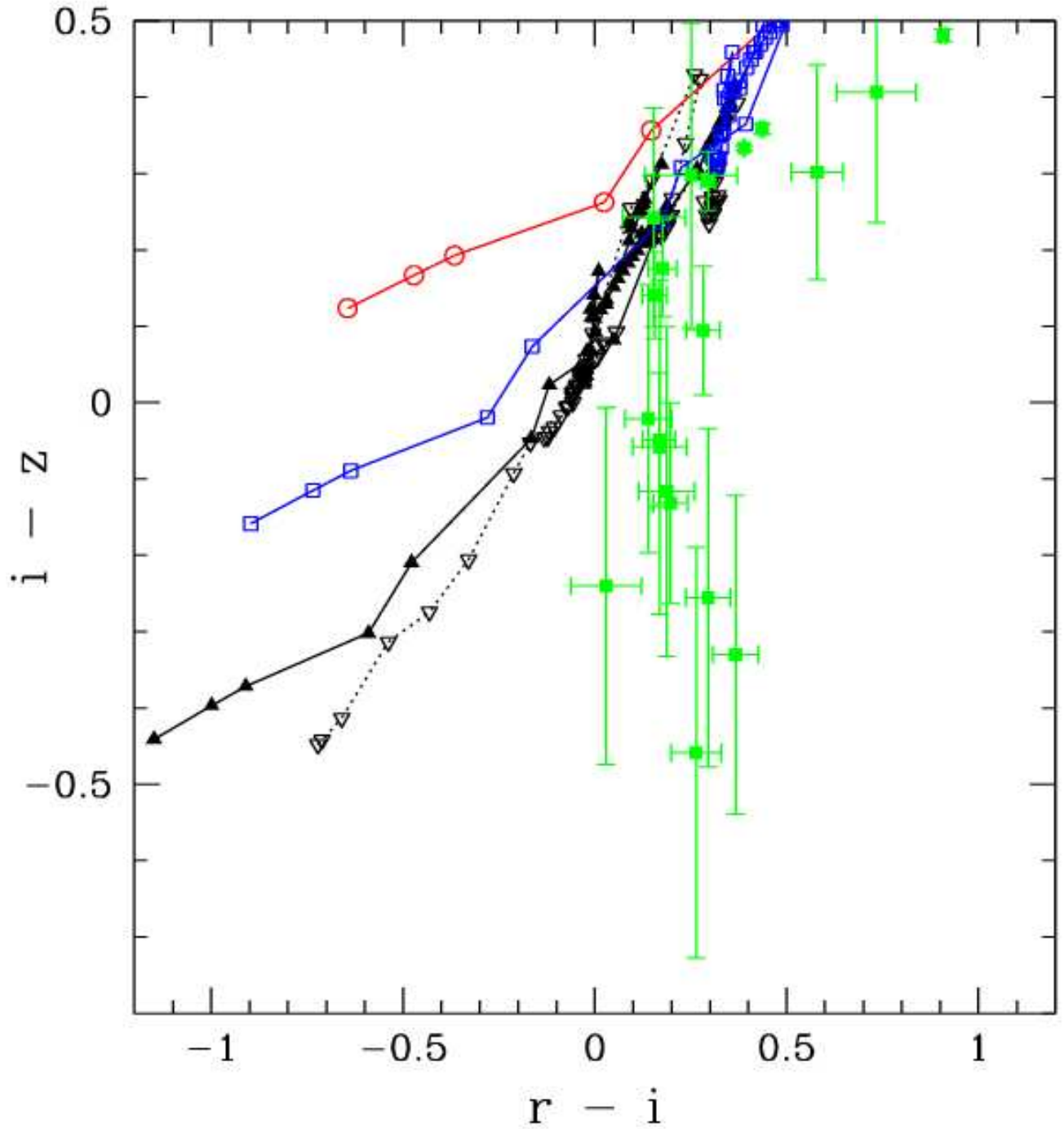
Fig. 26.— The green triangles show the population synthesis model with E(B-V) = 0, the blue squares show E(B-V) = 0.5, and the red squares show E(B-V) = 1.0. The model ages start at an age of 1 Myr, then increase by 1 Myr steps to 20 Myr, then by 5 Myr steps to 50 Myr, then 10 Myr steps to 100 Myr, 100 Myr steps to 1 Gyr, and 500 Myr steps to 10 Gyr. The clumps from Arp 107 are labeled as in Figure 1.

REFERENCES

Abazajian, K., et al. 2003, AJ, 126, 2081

Arp, H. 1966, Atlas of Peculiar Galaxies (Pasadena: Caltech)

Fazio, G. G., et al. 2004, ApJS, 154, 10

Hancock, M., Smith, B. J., Struck, C., Giroux, M. L., & Hurlock, S. 2009, AJ, 137, 4643

Hancock, M., Smith, B. J., Struck, C., Giroux, M. L., Appleton, P. N., Charmandaris, V., & Reach, W. T. 2007, AJ, 133, 676

Keel, W. C., Kennicutt, R. C., Jr., Hummel, E., & van der Hulst, J. M. 1985, AJ, 90, 708

Leitherer, C., et al. 1999, ApJS, 123, 3

Smith, B. J., Struck, C., Appleton, P. N., Charmandaris, V., Reach, W. & Eitter, J. J. 2005, AJ, 130, 2117

Smith, B. J., Struck, C., Hancock, M., Appleton, P. N., Charmandaris, V. & Reach, W. 2007, AJ, 133, 791

Smith, B. J., Struck, C., Hancock, M., Giroux, M. L., Appleton, P. N., Charmandaris V., Reach, W., Hurlock, S., & Hwang, J. 2008, AJ135, 2406

Struck, C. 1999, Phys. Rep., 321, 1

Smith, B. J., Giroux, M. L., Struck, C., Hancock, M. & Hurlock, S. 2010, AJ

Vazquez, G. A., & Leitherer, C. 2005, ApJ, 621, 695

Wallin, J. F., 1990, AJ, 100, 1477